J. Fluid Mech. (1984), *vol.* 144, *pp.* 329–362
Printed in Great Britain

Axisymmetric Couette flow at large Taylor numbers

By A. A. TOWNSEND
Emmanuel College, Cambridge

(Received 23 September 1983)

Measurements have been made in flow between concentric cylinders with only the inner one rotating, for Reynolds numbers (based on flow gap) from 17000 to 120000, corresponding to Taylor numbers from 8×10^7 to 4×10^9. At the lower speeds (Reynolds numbers less than 30000), the large-scale motion consists of toroidal eddies, highly uniform in spacing and intensity and convected by a slow axial flow past fixed sensors. By synchronizing an external oscillator with the passage frequency, flow velocity and small-scale turbulent intensity may be sampled at defined stages of the passage cycle and averaged to provide maps of the velocity fields and the associated distributions of small-scale intensity and Reynolds stress.

At higher speeds, the passage of toroidal eddies becomes too irregular to establish the passage cycle, but, by comparing the velocity fluctuations from four inclined hot wires placed near the outer cylinder, the current location of large-scale flow separation from the outer cylinder can be approximately determined. Statistics of the temporal variations of the location show that the large-scale motion still approximates to the toroidal form, but that there are azimuthal variations of separation position and velocity that indicate a change from toroidal to helical eddies. Conditional averages of flow velocity and small-scale turbulent intensity, based on relative distance from the position of flow separation, are very similar in form and magnitude to phase-selected averages obtained at lower speeds.

The considerable changes in the large-scale motion that occur as the Reynolds number increases from 300 to 1200 times the critical value are believed to arise from increase in the 'turbulent Taylor number' of the central flow, based on variation of angular momentum and on the eddy diffusion coefficients for linear and angular momentum. Effects on the motion of the slow axial flow, always less than 1 % of the peripheral flow velocity, are also discussed.

1. Introduction

In a recent paper, Smith & Townsend (1983) described hot-wire measurements of velocity made in Couette flow between concentric cylinders for the 'unstable' configuration in which the outer cylinder is at rest. For Reynolds numbers (based on flow gap and surface speed of the inner cylinder) from 7000 to 30000, a substantial part of the motion consists of axisymmetric toroidal eddies uniformly spaced along the cylinder axis, confirming work by Gollub & Swinney (1975), Barcilon *et al.* (1979), Koschmieder (1979), Bouabdallah & Cognet (1980) and Di Prima & Swinney (1981). With increasing Reynolds number above 30000, the regularity of arrangement diminishes, and, at a Reynolds number of 100000, the large-scale circulations are neither axisymmetric nor uniformly spaced in the axial direction. Smith & Townsend suggested that the original toroids break into segments of length comparable to half

the circumference of the annular space, and they linked the change with the observed development of wall flows with characteristics similar to those of turbulent flow on plane surfaces. At the lower Reynolds numbers, the motion in the wall layers can be described as the sum of large-scale axial motion from the toroids and from elongated Görtler eddies of small diameter (see Barcilon *et al.* 1979). As the Reynolds number increases, the influence of flow curvature diminishes close to the wall and the Görtler eddies there are replaced by eddies similar to those in plane flows.

The work reported below aims to determine the structure of the toroidal eddies, both the velocity field and the field of associated small-scale turbulent intensity, and to trace the changes in the large-scale motion with increase in Reynolds number to values for which regularity of the structure is less obvious. These measurements and those of Smith & Townsend depend on the presence of a slow axial flow to convect the large-scale motions past fixed hot-wire anemometers, and, while that motion is both axisymmetric and closely periodic in the axial direction, the output from fixed sensors contains periodic components of frequency equal to the axial convection velocity divided by the periodic spacing of the toroids. By synchronizing an oscillator to the passage frequency, samples of flow quantities can be taken at specific times in the passage cycle and averaged over many cycles to map the velocity field of the toroidal eddies and the distribution of small-scale intensity within them. These conditional averages are similar to those obtained in mixing layers, jets, and wakes by forcing the laminar instability to synchronize with an external periodic perturbation (see e.g. Zaman & Husain 1980). A difference is the absence of any external perturbation, which is replaced by the well-defind periodic signal induced by the regular passage of the toroidal eddies past a stationary anemometer.

At the larger Reynolds numbers, it is not possible to synchronize an oscillator, and it is necessary to find another way of determining the velocity and position of the large-scale circulations that are the successors of the toroids. The method adopted uses four single hot wires placed close to the outer cylinder and equally spaced in a line parallel to the axis of rotation. If the positions of large-scale flow separation and reattachment from the outer cylinder always lie within the span of the wire array, it is possible to estimate the current position and velocity of the circulation, and the information may be used in two ways. The statistics of position and velocity give information about the large-scale velocity pattern near the outer cylinder and its temporal changes, and the position of separation may be used as a sampling condition to map the velocity and turbulent intensity fields associated with the large-scale circulations.

One reason for study of the changes in large-scale structure of the Couette flow is that, at first acquaintance, they seem to contradict the well-established result in nearly unidirectional turbulent flows, that the large-scale tubulent motion is (statistically) geometrically similar for all Reynolds numbers more than about ten times the critical value for laminar instability. In the axisymmetric Couette flow, considerable changes occur for Reynolds numbers over the range from 300 to 1000 times the critical value. The reason is that the dynamics of the turbulent motion depend both on the friction velocity, which sets the level of velocity fluctuations, and on the flow velocity, which sets the level of curvature effects on the motion. The ratio of friction velocity to mean-flow velocity in the annulus decreases with increase of Reynolds number, and that may be regarded as the basic cause of the changes in flow structure.

2. Experimental arrangements

The flow is set up in the annular space between concentric cylinders of radii 152.4 mm and 229 mm with the inner cylinder rotating at angular speeds up to 24 rev/s. The inner cylinder is 1.80 m long and closely cylindrical in form, the outer one 1.85 m long and departing from the true cylindrical shape in places by 1 or 2 mm. The ends of the annular space are partially closed by attaching to the inner cylinder circular diaphragms of radii 5 mm and 10 mm less than the (mean) radius of the outer cylinder. With the unequal blockage of the ends, a slow axial flow is induced, never more than 0.5 % of the peripheral velocity of the inner cylinder, which has the effect of convecting the axisymmetric toroidal eddies along the annulus with uniform velocity. If the eddies remain unchanged in structure during the passage, the temporal variations recorded by a fixed velocity sensor can be used to determine the instantaneous spatial distributions in the axial direction.

For all the measurements, four hot-wire anemometers were placed at intervals of 44 mm in a line parallel to the axis at 10 mm from the outer cylinder. They were inclined at 45° to the direction of mean flow to be nearly responsive to the sum of the axial and peripheral (azimuthal) velocity fluctuations, and their purpose was to provide data for the establishment of the character and current location of the large-scale velocity field near the outer cylinder.

Dual hot wires of X-form, responsive to the streamwise and one transverse component of velocity, could be traversed radially in the diametral plane bisecting the row of wall wires and in a radial direction 45° downstream of them. The supports had a diameter of 3 mm, and pointed to the axis of rotation.

The anemometers were operated in the constant-temperature mode at overheat ratios of approximately 1.5, with the outputs amplified by circuits with uniform response from zero frequency to at least 5 kHz. The outputs were not linearized. A small wind tunnel was used for calibration, using steady flow speeds from 1.5 m/s to 10 m/s, with the inclination of the wires to the flow adjustable from $-15°$ to $+15°$. The air temperature of the calibration tunnel could be varied, and, from the wire response to temperature, the anemometer output voltages were corrected for departures of air temperature from 20 °C. In use, similar corrections were made to the output before using the wire calibration.

No calibrations were made for the wall wires, whose output fluctuations were normalized to unit variance, using values calculated from the data recorded on magnetic tape for the particular run. For these and some other recordings of the anemometer outputs, the signals were passed first through low-pass resistance–capacity filters to reduce contributions from small-scale motions.

For measurements with the phase-locked oscillator, the run durations were over 64 passage cycles, from approximately 15 min at the lowest speed to 5 min at the highest practicable speed, 10 rev/s or $R_e = 48000$. Magnetic-tape recordings were made over periods of approximately 1 min for the highest speeds, 20–24 rev/s, and 2 min for speeds around 10 rev/s.

3. Notation

The flow is described in terms of cylindrical polar coordinates; $r \equiv$ distance from the axis of rotation, $\theta \equiv$ azimuthal angle, and $y \equiv$ distance from the central diametral plane of the cylinders. The velocity components are respectively w, $U+u$, $V+v$, where U and V are mean values and functions of radial position. Then

U_1 is the peripheral velocity of the inner cylinder,

R_1, R_2 are the radii of the inner and outer cylinders,
$d = R_2 - R_1$ is the flow width,
$z = r - R_1$ is distance from the inner cylinder,
$R_e = U_1 d/\nu$ is the flow Reynolds number,
$T = 0.4R_e^2$ is the flow Taylor number for a radius ratio of 1.5,
T^* is the ratio of the Taylor number to the critical value for the first instability of the laminar flow (2335),
τ_1, τ_2 are the (kinematic) stresses on the inner and outer cylinders,
$2\pi G = 2\pi\tau_1 R_1^2 = 2\pi\tau_2 R_2^2$ is the kinematic transmitted torque per unit length,
$C_f = G/(U_1 R_1)^2$ is the friction coefficient,
V_c is the axial convection velocity of the axisymmetric eddies,
Ω_c is the circumferential convection velocity of large-scale velocity patterns,
$A(t)$ is the complex Fourier amplitude (equation 4.1),
$Q(\tau)$ is the covariance of $A(t)$,
$R(\tau) = Q(\tau)/Q(0)$ is the autocorrelation of $A(t)$,
ϕ is the cycle phase, either that of the passage cycle or that of the complex Fourier amplitude,
λ is the axial period of the toroidal eddies,
ϵ is the rate of energy dissipation per unit mass,
k_c is a critical wavenumber, separating eddies influenced by from those unaffected by flow curvature.

All the quantities are in the kinematic form, i.e. the mechanical values divided by the fluid density. The results are given in non-dimensional form, using U_1 and R_1 as the scales. An exception is radial position, expressed as a fraction of the flow width d.

Two equations for the flow may be quoted. The first expresses the constancy of angular momentum flux:

$$G = \overline{uw}\, r^2 - \nu r^3 \frac{\partial (U/r)}{\partial r}. \tag{3.1}$$

The mean value is taken, in principle, over cylindrical surfaces of constant radius and large axial extent, but, in practice, over a time interval long compared with the time for a toroidal eddy to pass the fixed sensor. The second is the equation for variation of the axial component of flow angular momentum, following a fluid particle:

$$\frac{D((U+u)\, r)}{Dt} = -\frac{\partial p}{\partial \theta} + \nu \frac{\partial}{\partial r}\left(r^2 \frac{\partial}{\partial r}\left(\frac{U+u}{r} \right) \right). \tag{3.2}$$

For flows with negligible pressure gradients in the flow direction, angular momentum remains constant during transport, except for the effect of viscous forces.

4. Analysis of anemometer data

The analysis of the anemometer outputs was made on the assumption, confirmed by the subsequent results, that there are present well-defined large-scale flow patterns spanning the annular gap and of considerable extent in the flow and axial directions. For Reynolds numbers less than 30000 (Taylor-number ratios less than 150000), they approximate closely to axisymmetric toroidal eddies encircling the inner cylinder and uniformly spaced along the axis of rotation. Since the axial drift carries them past fixed anemometers with convection velocities no more than 0.5 % of the peripheral flow velocity, their velocity fields generate fluctuations at frequencies much less than

Reynolds number	Period (mm)	λ/d	V_c/U_1
13570	164	2.15	0.0032
16900	150	1.96	0.0030
23700	157	2.07	0.0031
33300	145	1.90	0.0029
48100	142	1.86	0.0026
68100	139	1.82	0.0027
33000	148	1.94	0.00110
47800	143	1.88	0.00096
71200	132	1.73	0.00099

TABLE 1. Spacing and convection velocities of toroidal eddies

those from the small-scale turbulence convected past at the much higher flow velocity. By measuring the anemometer outputs after passage through suitable high- and low-pass filters (for details see Smith & Townsend 1982), the contributions to turbulent intensity and Reynolds stress from the axisymmetric motion and from the remaining motion can be found.

Results from the use of filters give information only about the mean-square variations of toroidal velocity at fixed radial positions. More detail can be found by using the well-defined frequency of passage of the toroids past a fixed sensor to synchronize a variable frequency oscillator in a phase-lock loop. It is then possible to sample velocity and small-scale turbulent intensity at defined stages of the passage cycle, to accumulate the samples over many cycles, and so to map the velocity fields and the associated intensity and stress fields of the toroidal eddies.† The technique is very similar to that used by many workers on large-scale flow patterns in turbulent flows. Most of them force transition of the laminar flow by external periodic forces and then obtain by a similar process of phase averaging maps of velocity and intensity fields. The differences are that here no external disturbance is used and that the flows are fully developed and turbulent at Reynolds numbers hundreds of times the value for first instability of the laminar flow.

A first use of the technique was to compare phase-averaged velocities from the four wall wires, sampling at eight stages of the passage cycle and accumulating the sums over 64 cycles. The variations of the averages over the passage cycle were analysed into Fourier components, and it was found that the phase of the first harmonic increased linearly with axial position of the wire. From the rate of phase advance, the spatial period may be calculated, and the results are given in table 1.

As the Reynolds number increases beyond 30000, the passage frequency becomes increasingly less well defined, and accurate synchronization with an external oscillator is not possible. Although the large-scale patterns are no longer axisymmetric, they remain similar to those of the toroids over circumferential ranges of $\frac{1}{2}\pi$ and axial distances of 150–200 mm. The local velocity and location of the pattern near the outer wall may be found approximately by forming the complex 'Fourier' amplitude,

$$A(t) = \sum_{n=1}^{4} v(y_n, t) \exp(\mathrm{i}k_0 y_n), \tag{4.1}$$

† To convert variations of flow quantities with time to variations with axial position, it is necessary to assume that the axial convection velocity remains the same during the passage cycle. Evidence for constant convection velocity is to be found in figure 1(*c*), which shows that the spatial phase of the large-scale velocity distribution at the other cylinder varies linearly with elapsed time.

where $v(y_n, t)$ is the output from the wall wire at $y_n = (n-\frac{5}{2})\,\delta$, and δ is the interval between wall wires (44 mm).

If the instantaneous distribution of v along the line of sensors is

$$v(y) = a\cos(ky-\phi)+f(y), \tag{4.2}$$

where $f(y)$ represents irregular contributions from smaller-scale motions without long-range order, then the complex amplitude is

$$A(t) = \tfrac{1}{2}a\,\mathrm{e}^{\mathrm{i}\phi}\left[\frac{\sin\{2(k-k_0)\,\delta\}}{\sin\{\frac{1}{2}(k-k_0)\,\delta\}}\right]+\tfrac{1}{2}a\,\mathrm{e}^{-\mathrm{i}\phi}\left[\frac{\sin\{2(k+k_0)\,\delta\}}{\sin\{\frac{1}{2}(k+k_0)\,\delta\}}\right]+\sum_{n=1}^{4} f(y_n)\exp(\mathrm{i}k_0 y_n). \tag{4.3}$$

For $k = k_0 = \pi/2\delta$ and $f(y) = 0$,

$$A(t) = 2a\exp(\mathrm{i}\phi) \tag{4.4}$$

and defines the current amplitude and phase (i.e. location of maxima) of v. In the experiment, a value for k of $\frac{1}{75}\pi$ mm^{-1} was assumed (a periodic spacing of 150 mm). If $k = k_0$,

$$A(t) = 2a\,\mathrm{e}^{\mathrm{i}\phi}+\tfrac{1}{2}a\frac{\sin(4k\delta)}{\sin k\delta}\mathrm{e}^{-\mathrm{i}\phi}+\sum_{n=1}^{4} f(y_n)\exp(\mathrm{i}k_0 y_n). \tag{4.5}$$

If phases of the wall pattern are calculated as the imaginary part of ln A, the effect of the second term is to introduce systematic errors, with a compression of scale near $\phi = 0$ and an extension near $\phi = \frac{1}{2}\pi$. The last term describes motions uncorrelated with the large-scale motion, and it produces random errors in the phase whose effect is to reduce the measured amplitudes of velocity and intensity averages obtained by using the calculated value of the phase as a sampling condition.

The magnitude of the last, 'random-noise', term can be estimated from the complex covariance of $A(t)$:

$$Q(\tau) = \langle A(t)\,A^*(t+\tau)\rangle. \tag{4.6}$$

Writing $Q_s(\tau) = 4\langle a(t)\,a(t+\tau)\exp\mathrm{i}(\phi(t)-\phi(t+\tau))\rangle$, and $g(t) = \Sigma f(y_n, t)\exp\mathrm{i}(k_0 y_n)$,

$$Q(\tau) = \tfrac{1}{4}Q_s(\tau)\left[\frac{\sin\{2(k-k_0)\,\delta\}}{\sin\{\frac{1}{2}(k-k_0)\,\delta\}}\right]^2+\tfrac{1}{4}Q_s(-\tau)\left[\frac{\sin\{2(k+k_0)\,\delta\}}{\sin\{\frac{1}{2}(k+k_0)\,\delta\}}\right]^2+\langle g(t)\,g^*(t+\tau)\rangle, \tag{4.7}$$

supposing the 'noise' part of A to be statistically independent of the large-scale motion. The first average refers to the large-scale motion, and its variation with time delay is slow compared with that of the 'noise' correlation $\langle g(t)\,g^*(t+\tau)\rangle$. If the individual $f(y_n)$ are uncorrelated, the covariance will decrease from an initial value of

$$Q(0) = 4.2\langle a^2\rangle+\langle gg^*\rangle \tag{4.8}$$

to a value near $4.2\langle a^2\rangle$ for a time delay short compared with the timescale of the large-scale motion (for $k = k_0 = \frac{1}{75}\pi$ mm^{-1}).

The effect of the 'noise' on the measured value of a coherent variation may be calculated from the ratio of the two terms in the previous equation, by assuming that the noise contribution to $A(t)$ is normally distributed in the complex plane with variance $\langle g(t)\,g^*(t)\rangle = Q(0)-Q(\tau_s)$, where τ_s is a time delay sufficient for $\langle g(t)\,g^*(t+\tau)\rangle$ to become small, but not sufficient for an appreciable change in the large-scale component. To reduce effects from uncertainty in the calculated phase from 'noise', averages were found by weighting the samples with the absolute value of the complex amplitude as well as selecting sixteen ranges of apparent phase. Then a sampled

	Attenuation factor	
s	1st harmonic	2nd harmonic
0	1.000	1.000
0.2	0.982	0.924
0.4	0.924	0.734
0.6	0.836	0.535
0.8	0.738	0.384
1.0	0.548	0.281
1.2	0.572	0.211
1.4	0.509	0.164

TABLE 2. Noise attenuation of conditional averages

quantity varying with real phase as $\cos\phi$ will have its amplitude reduced by the random errors in phase by a factor of

$$F = 2\pi \Big/ \int_{-\infty}^{\infty}\int_{-\infty}^{\infty} ((1+sx)^2+s^2y^2)^{\frac{1}{2}} \exp[-\tfrac{1}{2}(x^2+y^2)]\,dx\,dy, \tag{4.9}$$

where $s^2 = R(0)/R(\tau_s)-1$.

Calculated values of the attenuation are given in table 2 for various values of the noise, for sampled quantities varying as the first and second harmonics of the phase ϕ.

For measurements using complex Fourier amplitudes, the intensity of the 'noise' component was reduced by two stages of smoothing. Before recording, the anemometer outputs were passed through filters of time constants between 6.8 ms and 22 ms, selected to given non-dimensional values near 0.8. The filtered outputs were sampled at intervals of 4 or 8 ms for recording in digital form on magnetic tape. Complex amplitudes were calculated from moving averages of the four wall signals over 16 consecutive samples, equivalent to averaging over non-dimensional times of about 8. As a result, frequencies over 0.6 are strongly attenuated and only the variations near the orbital frequency of $0.32U_1/R_1$ are passed relatively unchanged. Longer averaging would lead to excessive attenuation and to slow response of the amplitude to changes. With practicable averaging, values of s less than 0.6 are not possible, and the table shows that second harmonics are considerably attenuated by the effect of noise and that higher harmonics are lost.

For conditional sampling of velocities, the outputs from the X-wires were filtered in the same way before recording on magnetic tape, but no averaging was made of the recorded samples. For conditional sampling of 'small-scale turbulent intensities', the outputs passed through high-pass filters before addition and squaring circuits.

5. The complex autocorrelation

Figures 1–3 show some of the measurements of the complex autocorrelation $R(\tau)$, normalized so that $R(0) = (1, 0)$, as trajectories in the complex plane and as plots of the modulus and phase angle against time delay.† At the largest Reynolds numbers, the trajectory, after a rapid movement towards the origin, begins to trace out a

† The phase angles are expressed as fractions of 2π, and lie in the range -0.5–0.5; in radians, from $-\pi$ to π.

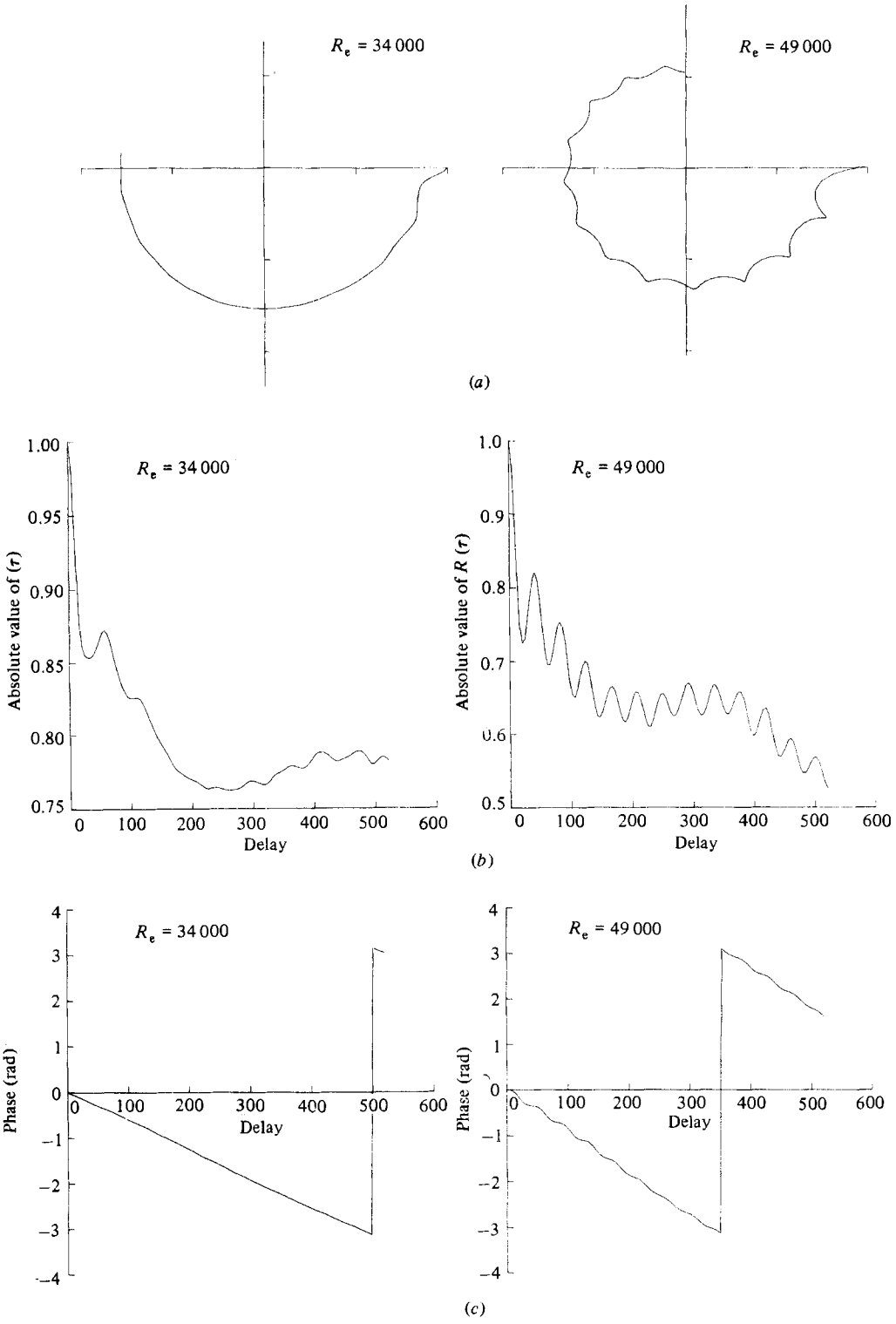

FIGURE 1. Autocorrelations of the complex amplitude for Reynolds numbers of 34000 and 49000 with $V_c/U_1 = 0.003$: (*a*) Trajectory in the complex plane; (*b*) absolute value *vs.* non-dimensional time delay; (*c*) phase angle *vs.* time delay.

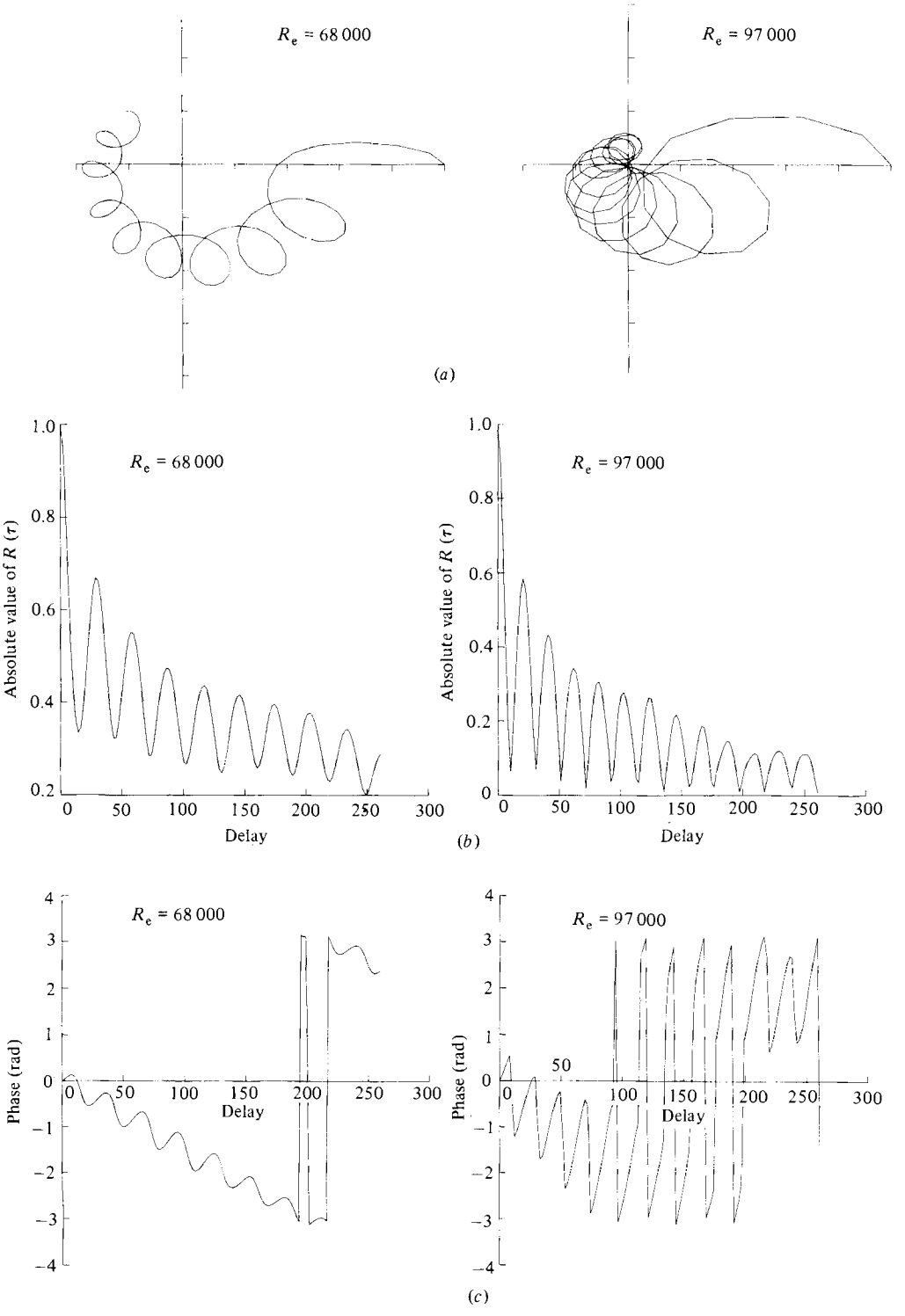

FIGURE 2. Autocorrelations of the complex amplitude for Reynolds numbers of 68000 and 97000 with $V_c/U_1 = 0.003$: (*a*) trajectory in the complex plane; (*b*) absolute value *vs.* non-dimensional time delay; (*c*) phase angle *vs.* time delay.

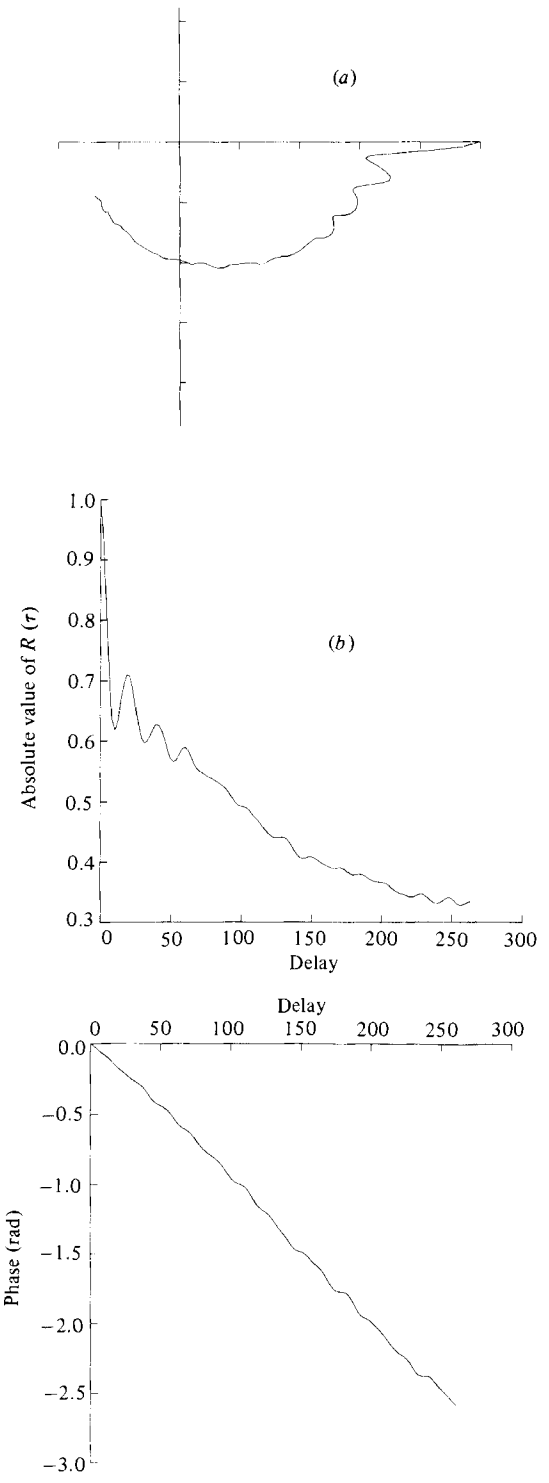

FIGURE 3. Autocorrelation of the complex amplitude for a Reynolds number of 97000 and for $V_c/U_1 = 0.001$; (*a*) trajectory in the complex plane; (*b*) absolute value *vs.* non-dimensional time delay; (*c*) phase angle *vs.* time delay. (Broken lines are v or w, numbers are gap ratios z/d.)

cycloidal path composed of an anticlockwise orbit of non-dimensional frequency near 0.30 and a smaller, clockwise orbit of frequency near 0.02. By itself, the clockwise orbit would indicate that the velocity field is helical in structure, produced by wall-velocity distributions of the form

$$v(y,\theta) = b\cos(ky-\theta) \tag{5.1}$$

convected circumferentially at the flow velocity near the centre of the annulus, where the angular velocity is $0.32U_1/R_1$.

A clockwise trajectory with non-dimensional frequency 0.02 could be produced by the axial convection at velocity V_c of toroidal eddies of form

$$v(y,\theta) = a\cos ky \tag{5.2}$$

(circumferential convection of axisymmetric flow patterns causes no velocity changes at a fixed sensor).

Superposition of the two orbits means that the large-scale flow is nearly composed of velocity distributions of the form

$$v(y,\theta) = a\cos ky + b\cos(ky-\theta) \tag{5.3}$$

convected with axial velocity V_c, and circumferential angular velocity Ω_c. Depending on the ratio a/b, the motion could be described either (i) as toroidal eddies inclined to the diametral plane and with an azimuthal modulation of velocity in quadrature with displacement of the eddy axis ($a \gg b$), or (ii) as nearly helical eddies with axial deviations from a true helix in quadrature with variation of velocity ($a \ll b$). In either case, the complex amplitude is (for $k = k_0 = \pi/2\delta$ and ignoring the 'noise' contribution)

$$A(t) = 2a\exp(\mathrm{i}kV_c t) + 2b\exp(\mathrm{i}(kV_c-\Omega_c)t), \tag{5.4}$$

and the covariance is

$$Q(\tau) = 4a^2\exp(-\mathrm{i}kV_c\tau) + 4b^2\exp(-\mathrm{i}(kV_c-\Omega_c)\tau). \tag{5.5}$$

By itself, the second term in (5.3) represents 'single-start' helical eddies, of sense the same as that of the mean-flow streamlines. That the sense depends on the axial flow was confirmed by interchanging the end diaphragms, so reversing the direction of axial flow, and observing that the trajectory became clockwise.

The simple doubly periodic form of (5.3) and (5.5) is valid only for moderate time delays, especially for the larger Reynolds numbers. Both components decrease in amplitude, and, at Reynolds numbers of 100000, the amplitude of the toroidal component is reduced by a factor of three for a non-dimensional time delay of 40, while the helical component has decreased by a factor nearer ten.

A few measurements have been made of autocorrelations with the axial velocity reduced from the standard value of nearly $0.003U_1$ to around $0.0010U_1$ (figure 3). Only for the largest Reynolds numbers are there clear variations at the orbital frequency, and the variations appear to be mostly of absolute value with little modulation of phase. For not too long delays, the autocorrelation of figure 3 is described approximately by

$$Q(\tau) = (4a^2 + 2b^2\cos(\Omega_c\tau))\exp(\mathrm{i}kV_c\tau), \tag{5.6}$$

which would be produced by velocity distributions of the form

$$v(y,\theta) = (a + b\cos\theta)\cos ky \tag{5.7}$$

convected with axial velocity V_c and angular velocity Ω_c.

6. Velocity fields of the large eddies

The conditional averages of the velocity fluctuations, based on the phase determined either from a phase-locked oscillator or from the complex amplitude $A(t)$, can be used to map the velocity field of the large eddies, reliably if the field is closely periodic in the axial direction but less so if the axial periodicity is imperfect. Figure 4 shows the variation with phase of conditionally averaged components of the velocity fluctuation, for a range of radial positions and for Reynolds numbers of 17000 and 97000. For the smaller Reynolds number, phase conditions for averaging were obtained from a synchronized oscillator and there is little uncertainty in the phase. Except near the flow boundaries, the averaged velocities vary nearly sinusoidally with phase, and the distributions may be described by

$$u = f(r)\sin(\phi-\phi_0), \quad v = \frac{C}{r}\cos(\phi-\phi_0)\cos\left(\frac{\pi z}{d}\right), \quad w = \frac{C}{r}\sin(\phi-\phi_0)\sin\left(\frac{\pi z}{d}\right), \tag{6.1}$$

where ϕ_0 is the reference phase of the run.

That is to say, the variations of u and w are nearly in phase at all radial stations, with the variation of v in quadrature and reversing in sign across the flow centre. The amplitudes of the u- and v-variations are small near the flow centre, while that of w is a maximum there, decreasing towards the flow boundaries.

If the velocity patterns are 'frozen' and convected unchanging past the sensors with velocity V_c, the axial distributions are obtained by substituting ky for ϕ in (6.1), where k is the wavenumber of the axial variation (approximately $\frac{1}{75}\pi$ mm^{-1}). At a Reynolds number of 35000 the autocorrelation (figure 1) shows that there is very little azimuthal variation of the large-scale structure, and the velocity distributions are nearly of the form

$$u = f(r)\sin ky, \quad v = \frac{C}{r}\cos\left(\frac{\pi z}{d}\right)\cos ky, \quad w = \frac{C}{r}\sin\left(\frac{\pi z}{d}\right)\sin ky. \tag{6.2}$$

Inspection of the cycle variations for the larger Reynolds number shows much less regularity. The sampling conditions were obtained from the phase of the complex amplitude, which is subject to considerable disturbance from intrusive, small-scale velocity fluctuations and from the probable variations in the effective wavenumber of the axial-velocity distribution (4.2). Particularly near the flow centre, the amplitudes of the axial and radial components are small compared with the azimuthal (streamwise) component, and the phases are most uncertain. With allowance for the various errors and uncertainties, it can be said that the cycle variations for $R_e = 97000$ are broadly similar to those for $R_e = 17000$, to the extent that the cycle phase of the v-variation reverses across the flow and that the variations of u near the boundaries and of w near the flow centre are similar and in quadrature with those of v.

The azimuthal variations are specified by the complex autocorrelation $Q(r)$, and, using the results of figure 2, the velocity distributions approximate to the form

$$\left.\begin{aligned} u &= f(r)\,(a\cos ky + b\cos(ky-\theta)), \\ v &= \frac{C}{r}\cos\left(\frac{\pi z}{d}\right)(a\cos ky + b\cos(ky-\theta)), \\ w &= \frac{C}{r}\sin\left(\frac{\pi z}{d}\right)(a\sin ky + b\sin(ky-\theta)). \end{aligned}\right\} \tag{6.3}$$

For the smaller Reynolds number, the velocities are nearly independent of angle, and they are convected past the sensor with the axial convection velocity V_c, i.e. $b \ll a$. At the larger Reynolds number, the velocities vary azimuthally as $a + b\cos\theta$, and they are convected with the angular convection velocity $\Omega_c \approx 0.32 U_1/R_1$.

Near the flow boundaries, variations of averaged radial component of velocity are not so closely sinusoidal, having peaked maxima of velocity directed away from the adjacent boundary and flat minima of velocity toward it. Ignoring the small contributions from the second harmonic, the velocity variations over the cycle may be specified by the amplitudes and phases of the first harmonics. Figure 5 shows the radial distributions of amplitude and phase for Reynolds numbers between 17000 and 97000, and the measurements are further summarized in figure 6, which shows the 'peak' amplitudes as a function of Reynolds number. For the radial component, the 'peak' amplitude is the value near the centre of the flow gap (at $z/d = 0.49$), but the maximum of the axial and azimuthal components occur near the cylinders and the values shown are amplitudes at $z/d = 0.87$ and $z/d = 0.99$. Also included are amplitudes calculated from measurements of the 'low-frequency' intensities obtained by high- and low-pass filtering, on the assumption that the (low-frequency) variation is sinusoidal and of constant amplitude. If the whole motion is in the form of regularly spaced, axisymmetric toroidal eddies, these amplitudes should agree with those from conditional averages.

As can be seen, there are considerable differences. First, the amplitudes from the filtered intensities become small for Reynolds numbers over 50000 since they do not include any contributions from components of orbital frequency. Next, observation of the phase-lock circuit and inspection of time records of the low-frequency fluctuations show that breaks in the regularity of eddy passage are appreciable at a Reynolds number of 34000 and become frequent for larger Reynolds numbers. With loss of register between the oscillator and the passing eddies, the sampling criterion becomes blurred and the measured amplitudes less than the true amplitudes of variation within the eddies. Finally, although averages based on phase of the complex amplitude are less affected by irregularity of eddy spacing, random errors in phase arise from the 'noise' of the small-scale eddies and from variation of the effective wavenumber.

Taking into account the possibilities of error, amplitudes from the three methods are consistent for the smaller Reynolds numbers, and the differences for Reynolds number near 50000 are no more than would be expected. Only the complex amplitude method can be used for the largest Reynolds numbers. Making use of table 2, the measured conditional averages are estimated to be less than the true values in ratios of approximately 0.85. With that in mind, the amplitudes are found to decrease with increase of Reynolds number, for the v- and w-components, possibly by a factor of 0.6 over the whole range. That factor is a little more than might be expected from the change in friction velocity, in a ratio of 0.80 if the friction coefficient varies as $R_c^{-\frac{1}{4}}$, and of 0.75 if it varies as $R_c^{-\frac{1}{3}}$.

The momentum flux carried by the large eddy motion is no more than $\frac{1}{3}$ of the total flux, and the circumferential velocity variations, though in phase with the radial variations, are small near the centre of the flow gap. That and the peaks in the variation of w (figure 4) suggest that the motive power of the motion lies within the wall layers and that the separating fluid coasts across the gap, conserving angular momentum and neither gaining nor losing much energy.

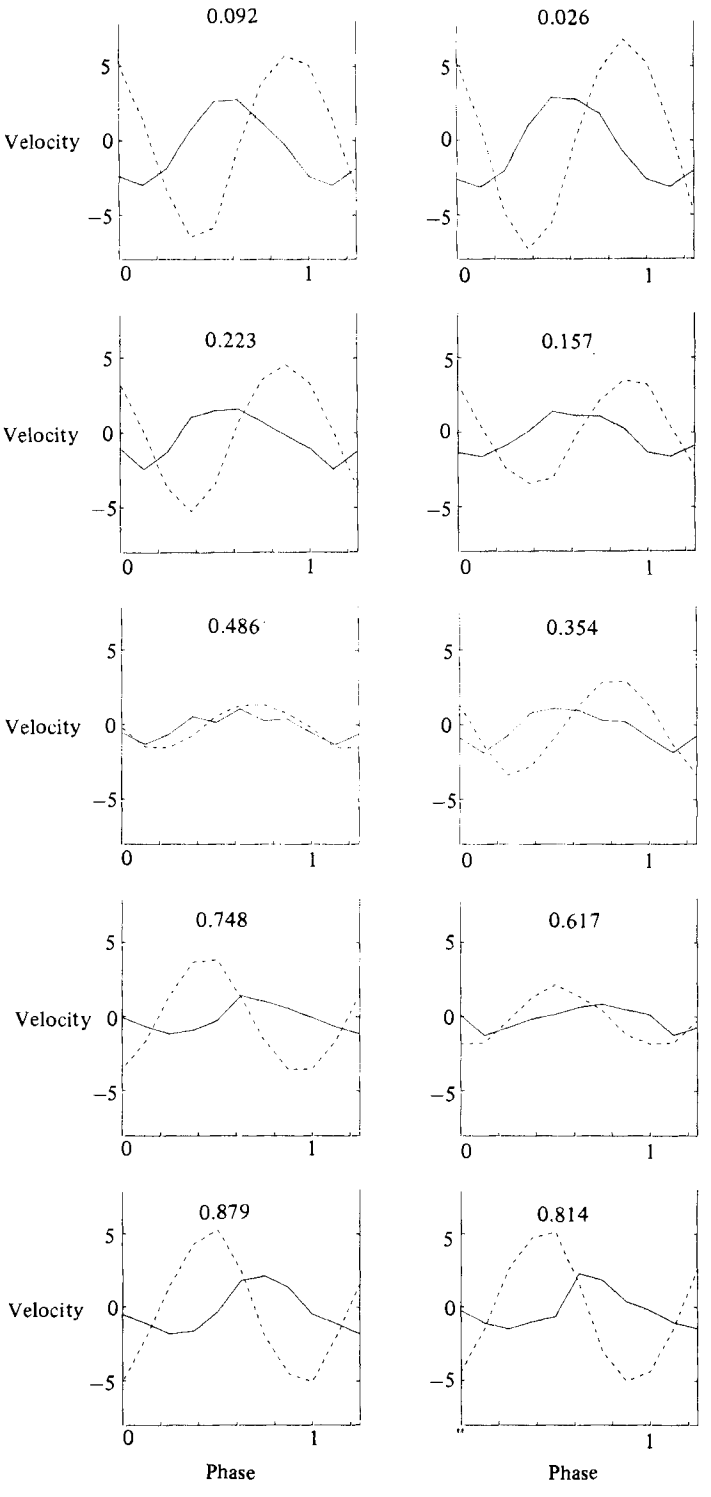

FIGURE 4(*a*). For caption see p. 345.

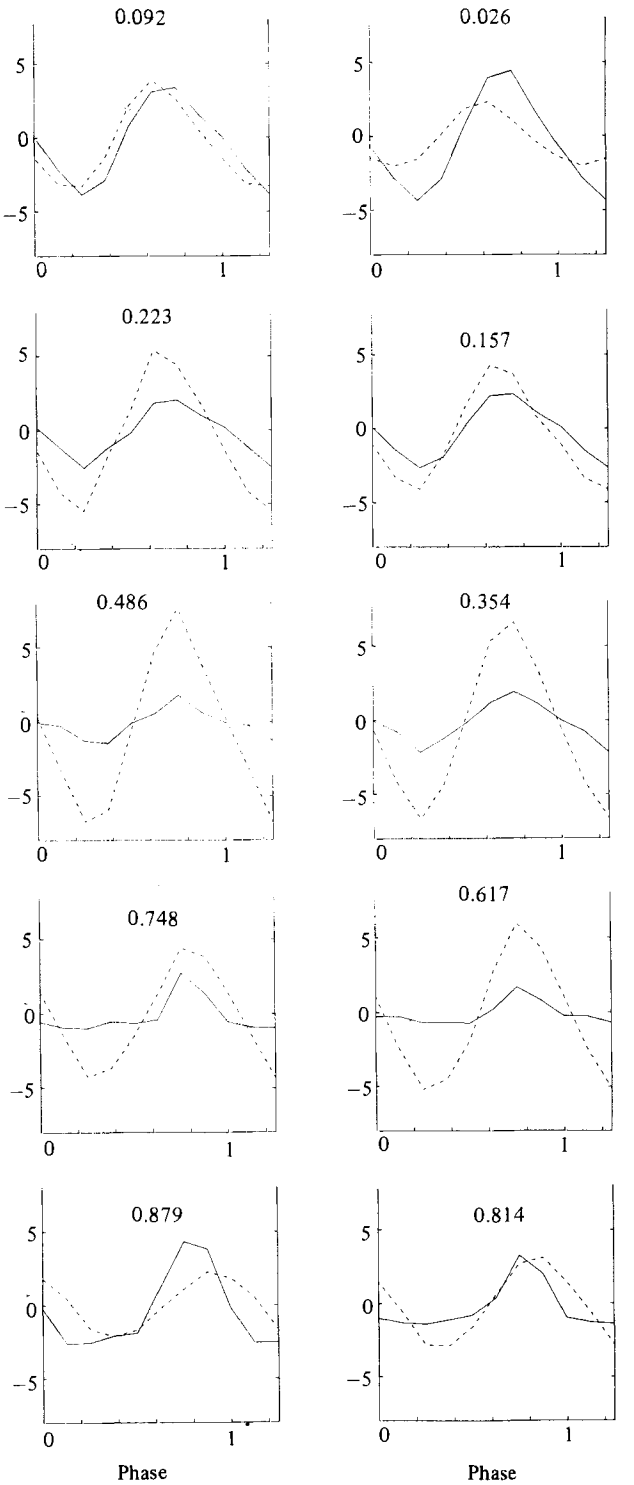

FIGURE 4(*a*). For caption see p. 345.

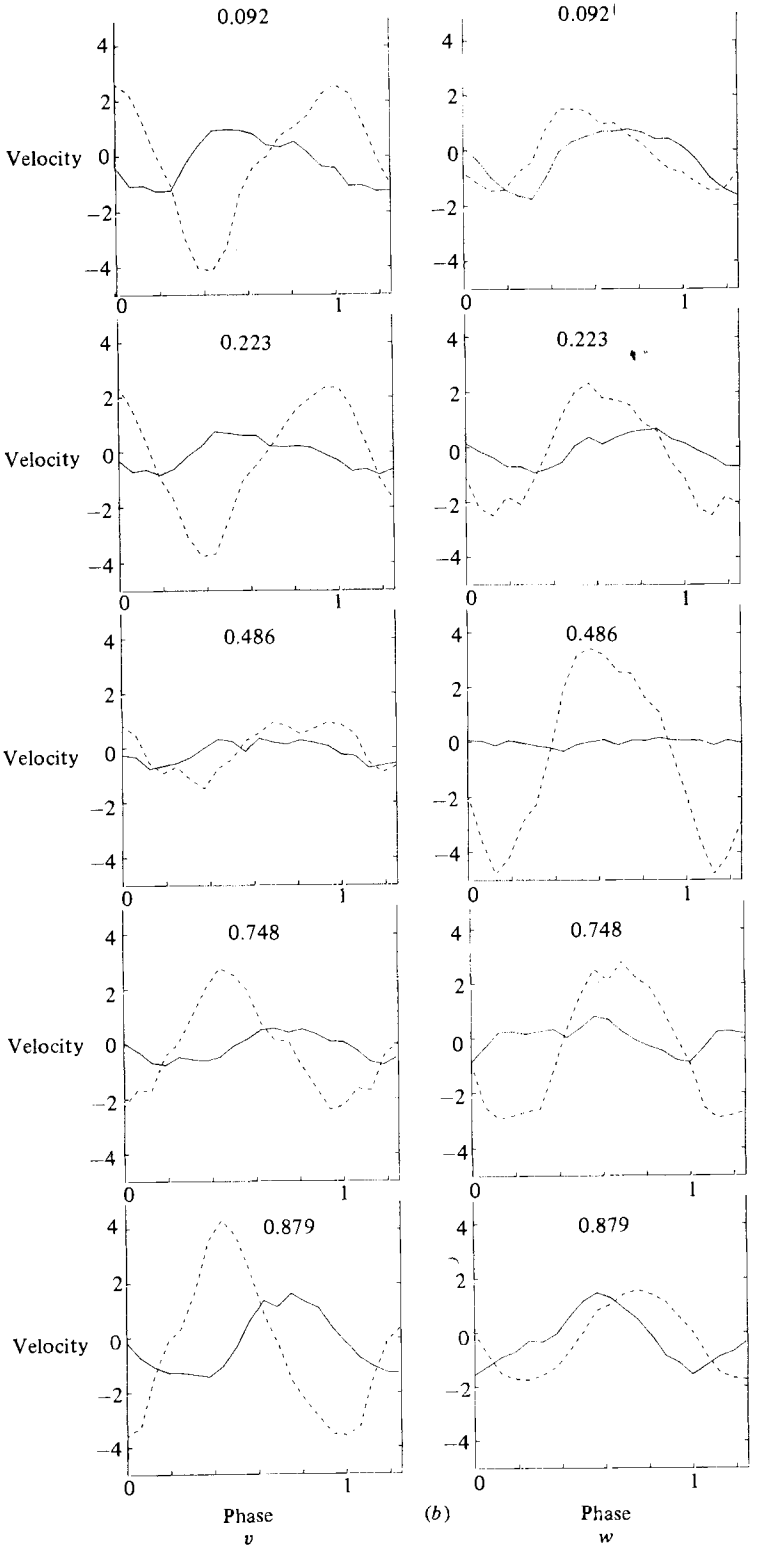

FIGURE 4(*b*). For caption see facing page.

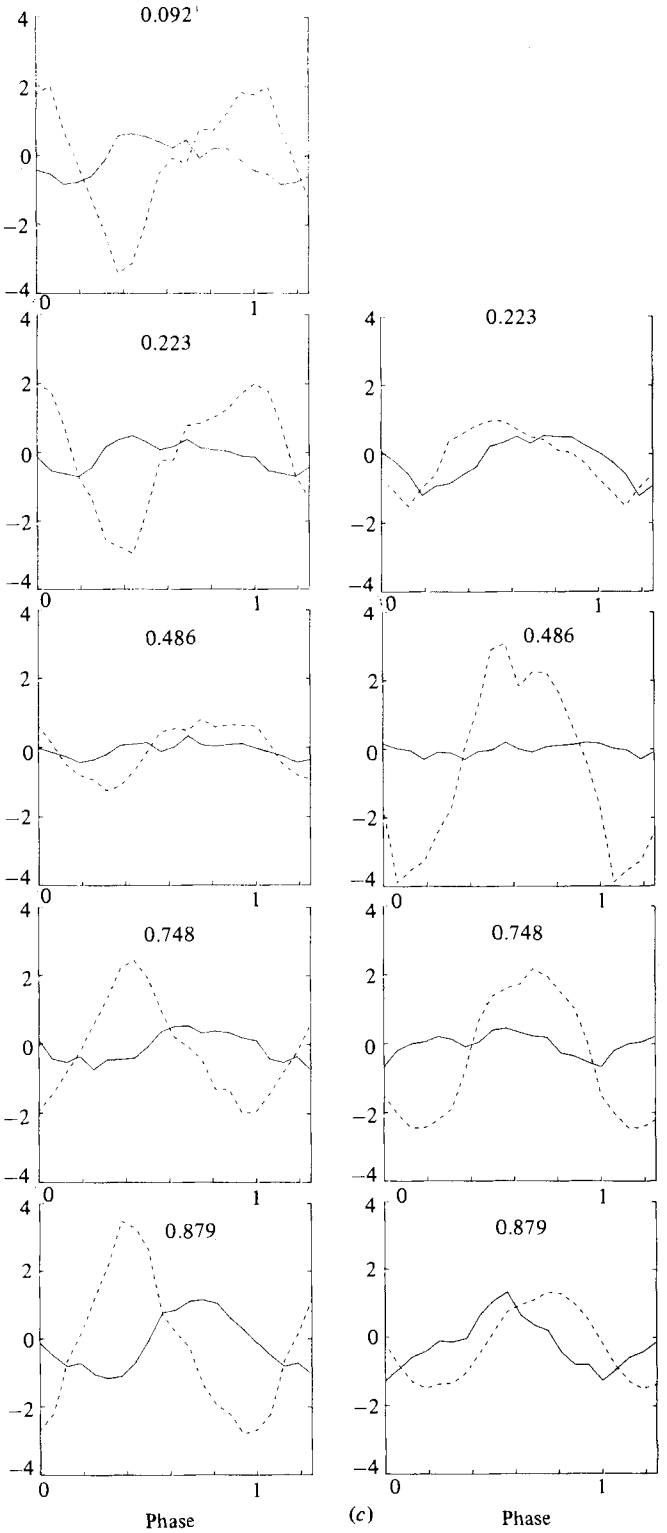

FIGURE 4. Conditional averages of flow velocity against cycle phase for a range of radial positions: (*a*) $R_e = 17000$ (phase-lock method); (*b*) $R_e = 68000$ (complex amplitude phases); (*c*) $R_e = 97000$ (complex amplitude phases).

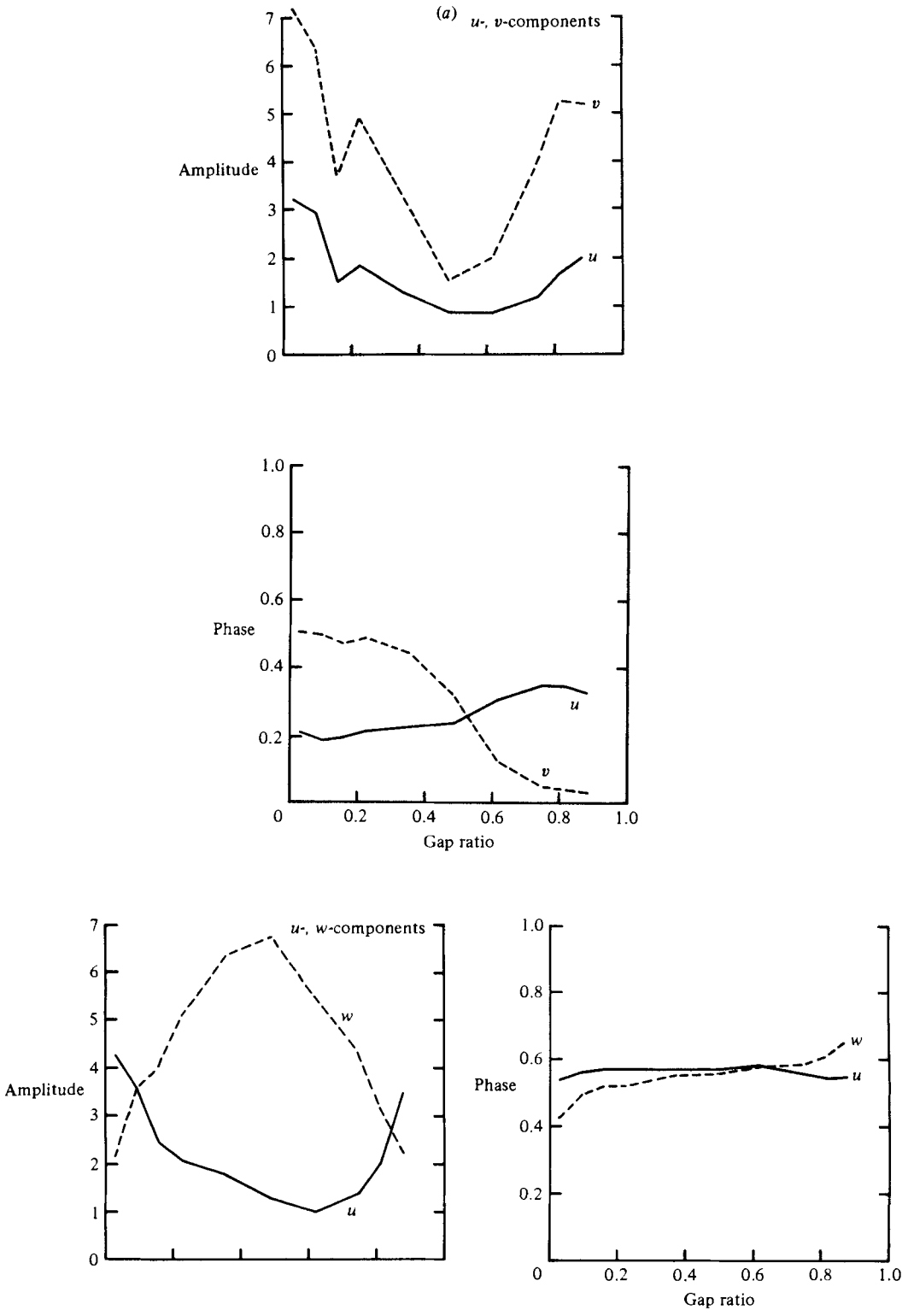

FIGURE 5(*a*). For caption see p. 351.

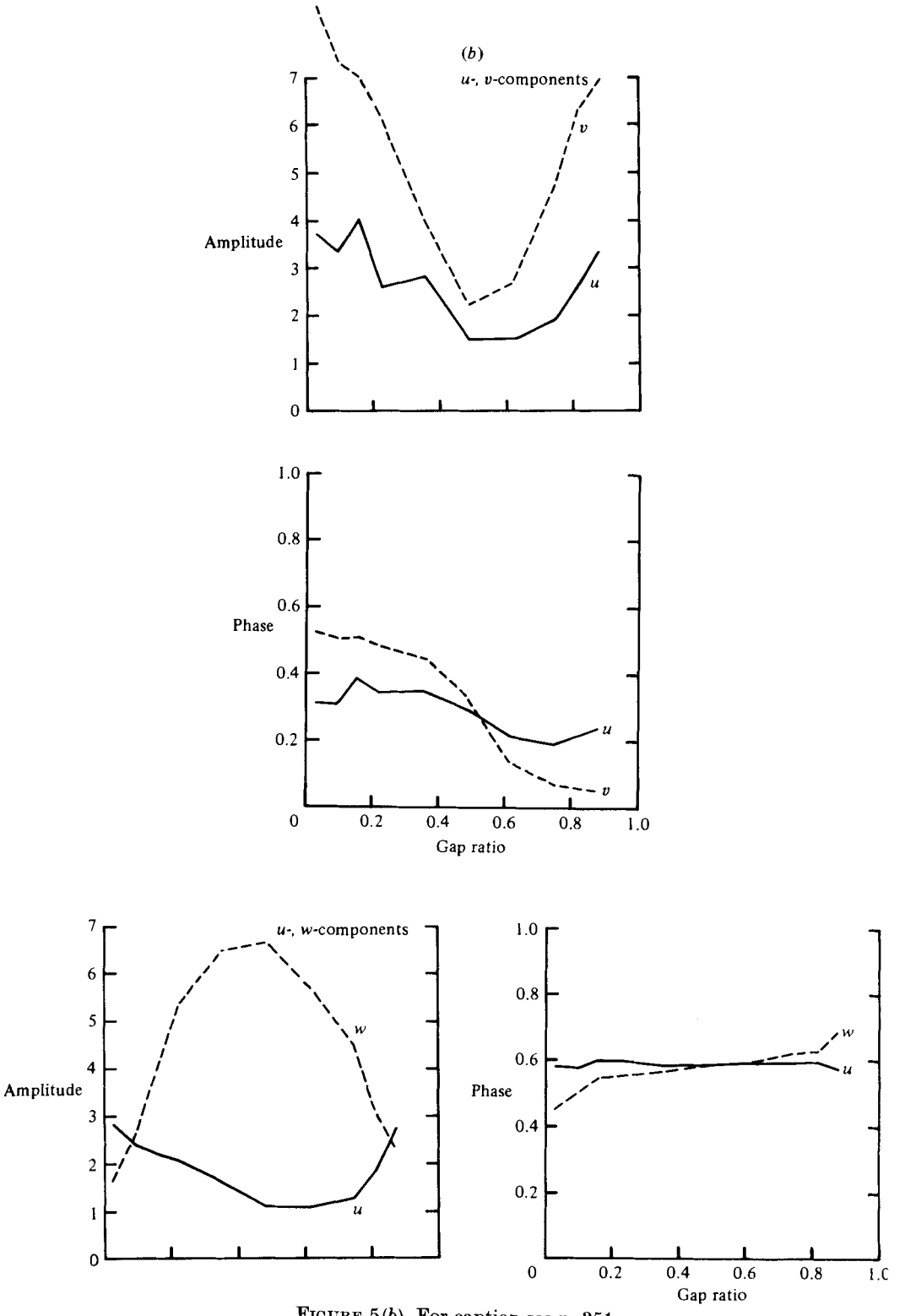

FIGURE 5(*b*). For caption see p. 351.

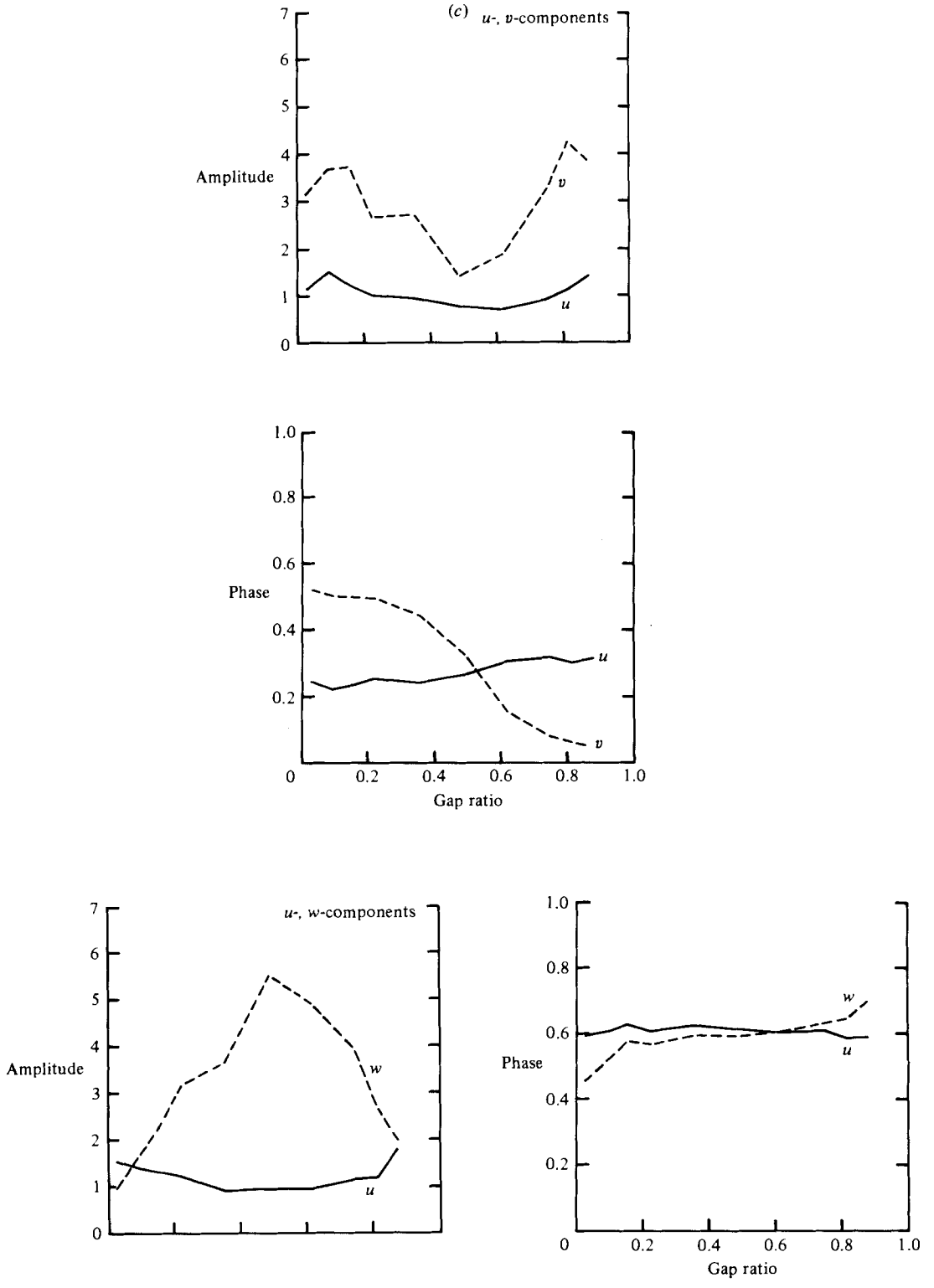

FIGURE 5(c). For caption see p. 351.

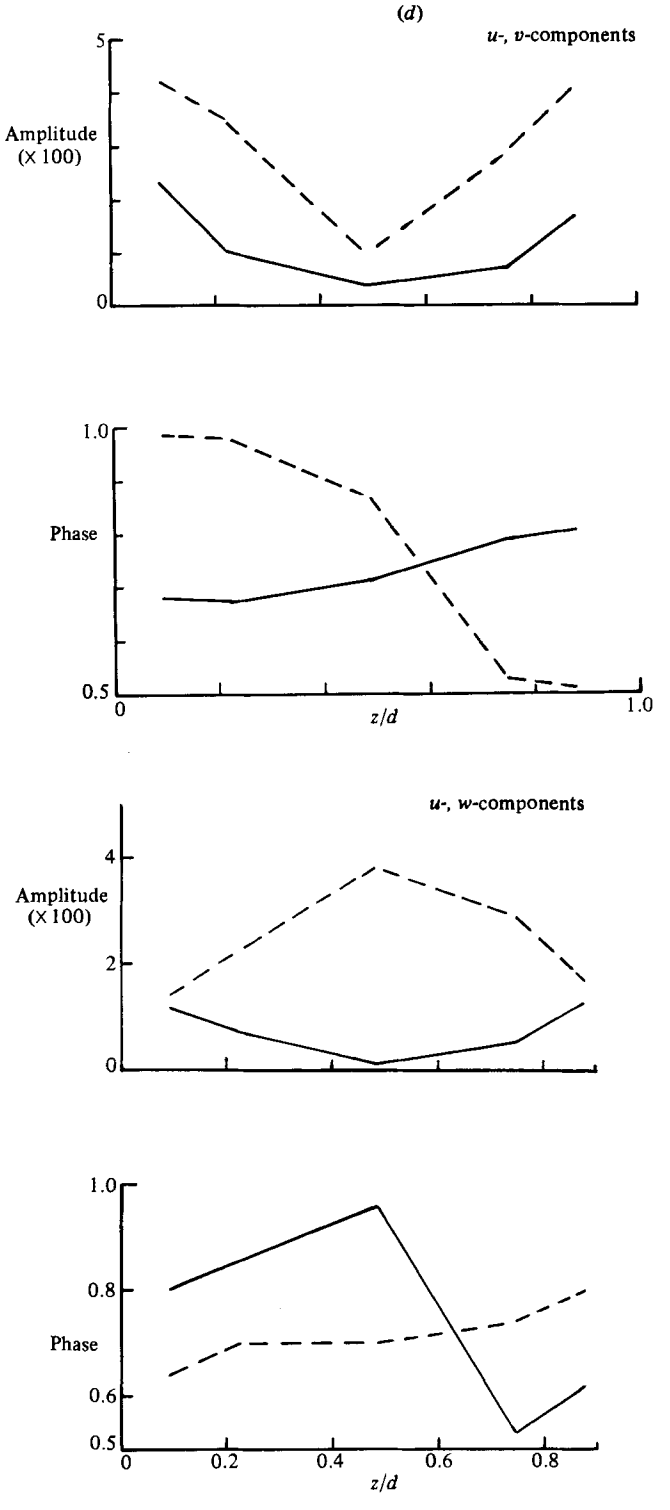

FIGURE 5(*d*). For caption see p. 351.

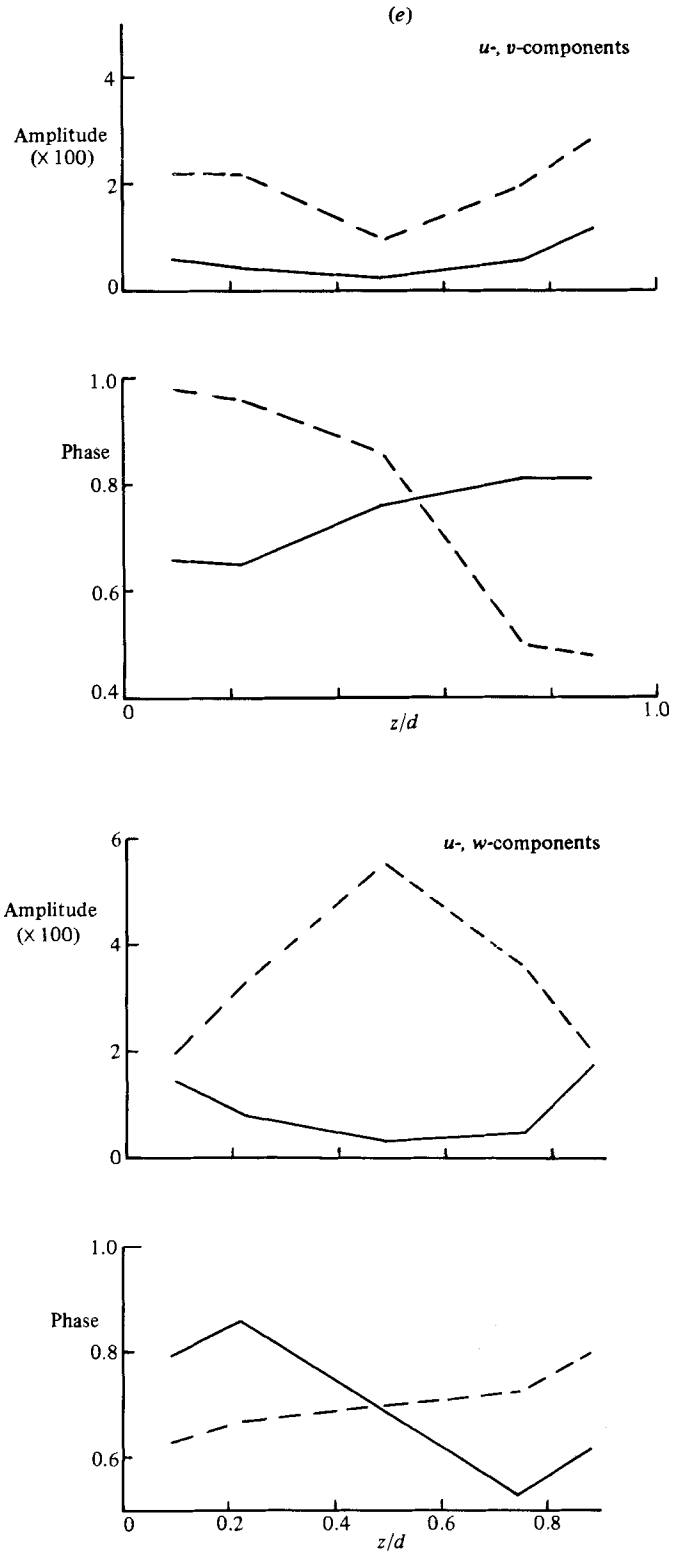

FIGURE 5(*e*). For caption see facing page.

(*f*)

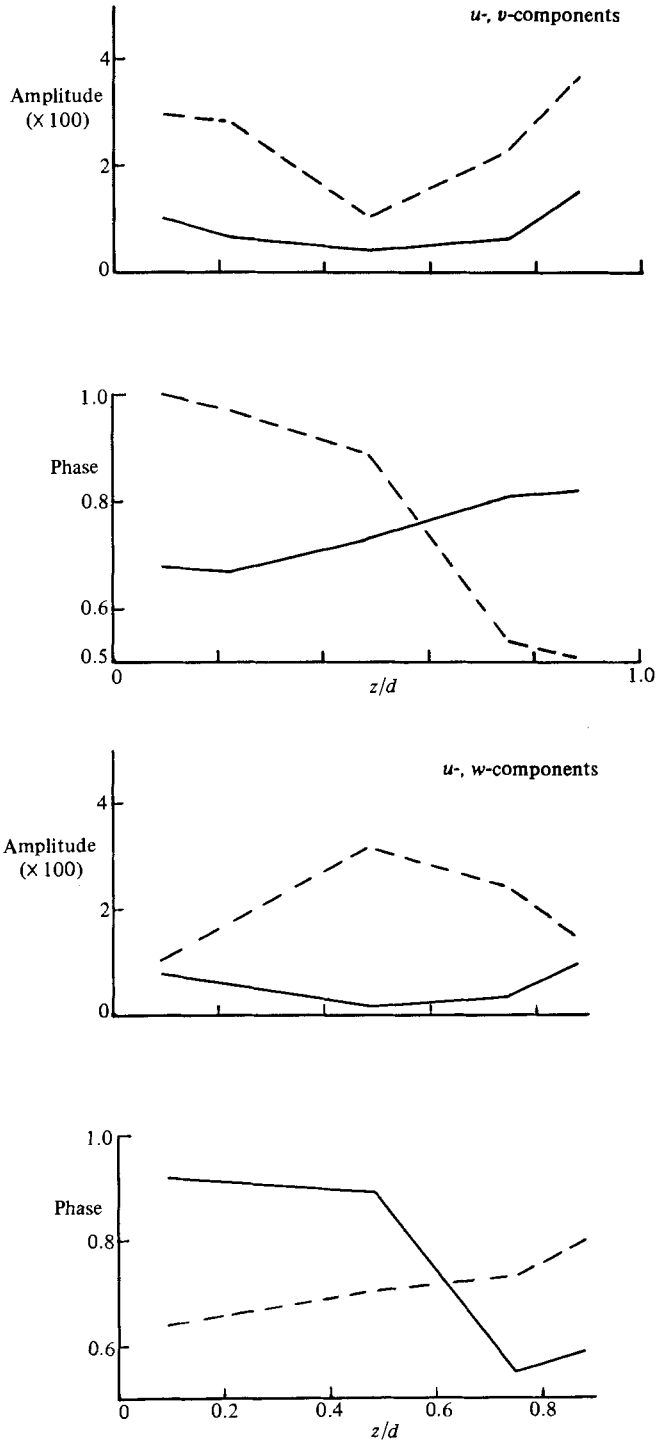

FIGURE 5. Radial variations in amplitude and phase of the first harmonics in the cyclic changes of conditionally averaged velocity: (*a*) $R_e = 17000$; (*b*) 24000; (*c*) 34000; (*d*) 48000; (*e*) 68000; (*f*) 97000. In (*a*) and (*b*) the phases are in radians; in the other figures they are in fractions of a period.

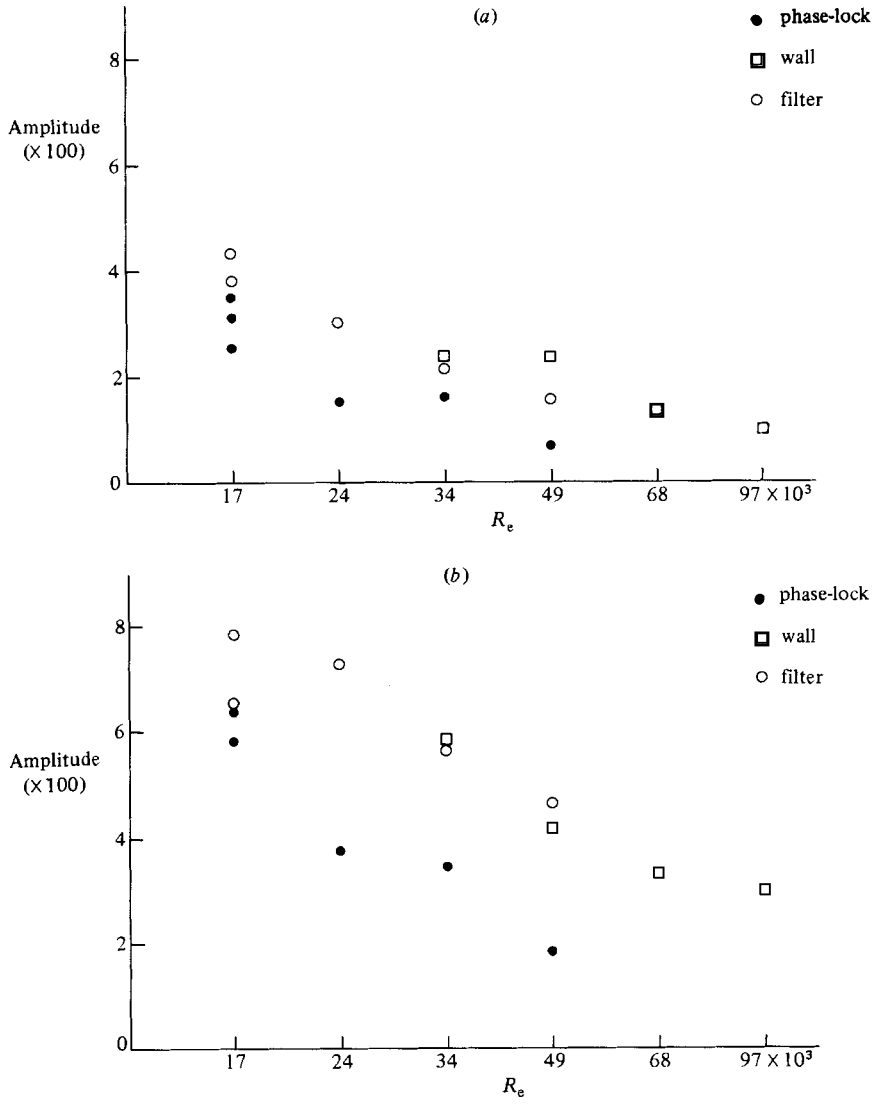

FIGURE 6(*a*,*b*). For caption see p. 353.

7. Distribution of small-scale turbulence in the large eddies

A clear distinction between the large-scale motion and the irregular turbulent motion is possible only if the large eddies are uniform both in velocity pattern and scale, so that the turbulent component appears as the residue after subtracting the coherent velocity field of the large eddies. Favourable conditions are approached for flows of Reynolds numbers less than 25000 for which records of low-frequency velocity fluctuations show the amplitude and period to be remarkably uniform. For the standard end conditions, the non-dimensional passage frequencies are about 0.019, and are attenuated by factors of 16 (more at lower Reynolds numbers) after passage through resistance-capacity high-pass filters of time constant 0.1 s (a non-dimensional time constant of 0.3 for $R_e = 25000$). The turbulent component has a broad spectrum with centroid near a non-dimensional frequency of 3, and it suffers little attenuation.

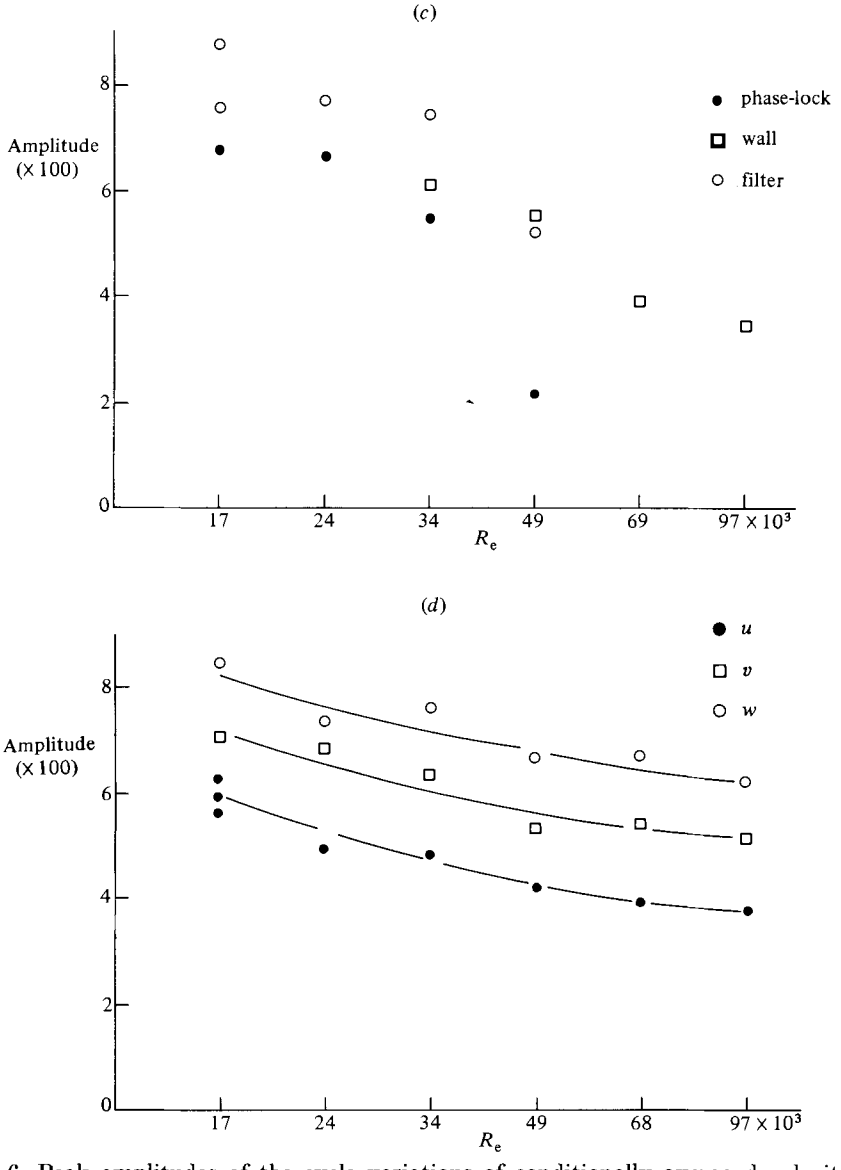

FIGURE 6. Peak amplitudes of the cycle variations of conditionally averaged velocity against Reynolds number: (*a*) u-component; (*b*) v-component; (*c*) w-component; □, complex amplitude phases); (*d*) 'peak amplitudes' of total velocity fluctuations, calculated as $(2\overline{u^2})^{\frac{1}{2}}$ etc., for the same radial positions.

Figure 7 shows the results of phase-sampling 'small-scale turbulent' intensities and stresses, using the phase-locked oscillator for $R_e = 17000$ and the complex amplitude for $R_e = 97000$ to provide sampling criteria for anemometer signals squared after passage through suitable high-pass filters.

For the smaller Reynolds numbers, mean values are in fair agreement with intensities of the 'high-frequency' component measured using the filter method. Characteristically, the maxima of intensity and Reynolds stress occur at positions of maximum radial velocity away from the nearer boundary, i.e. the phase of the variation reverses across the centre of the flow. Near the flow centre, the variations

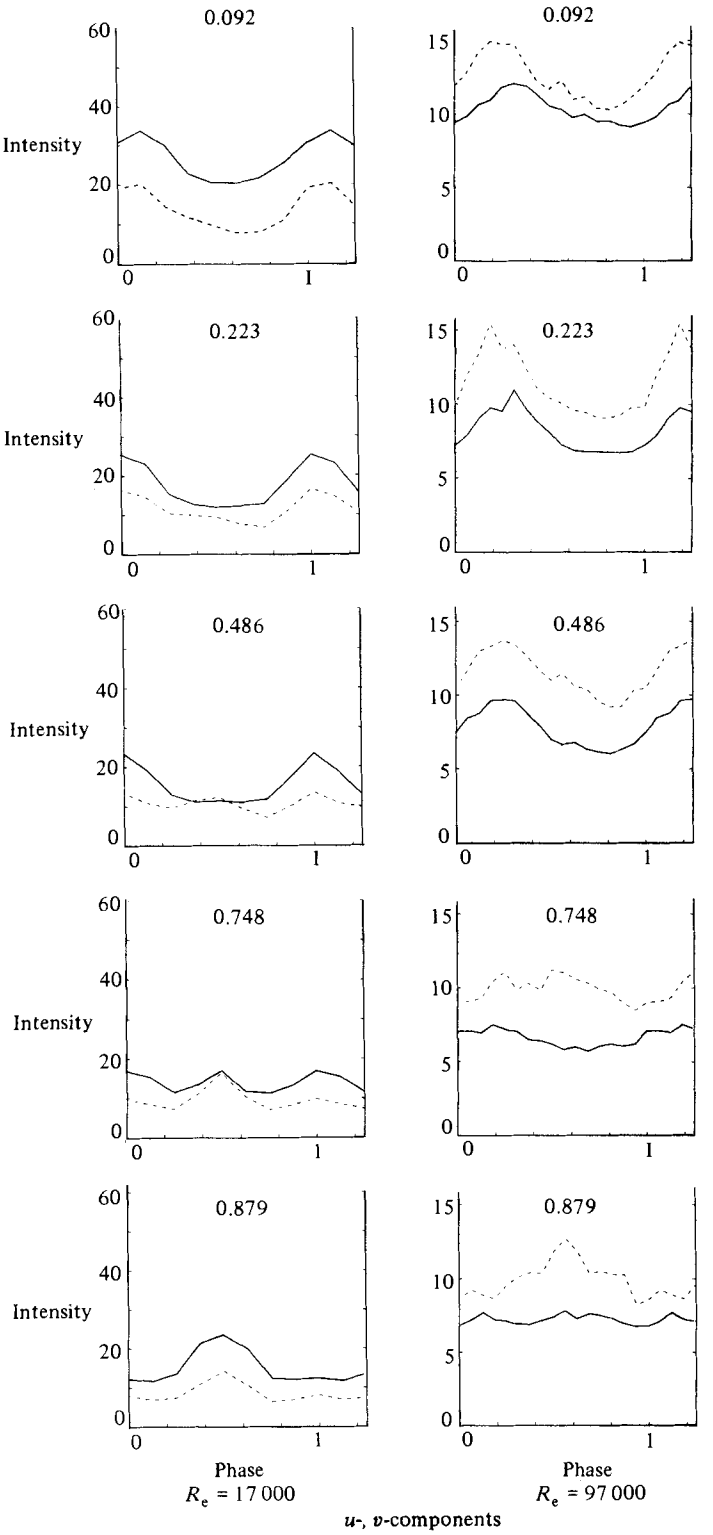

(*a*)

FIGURE 7(*a*). For caption see p. 356.

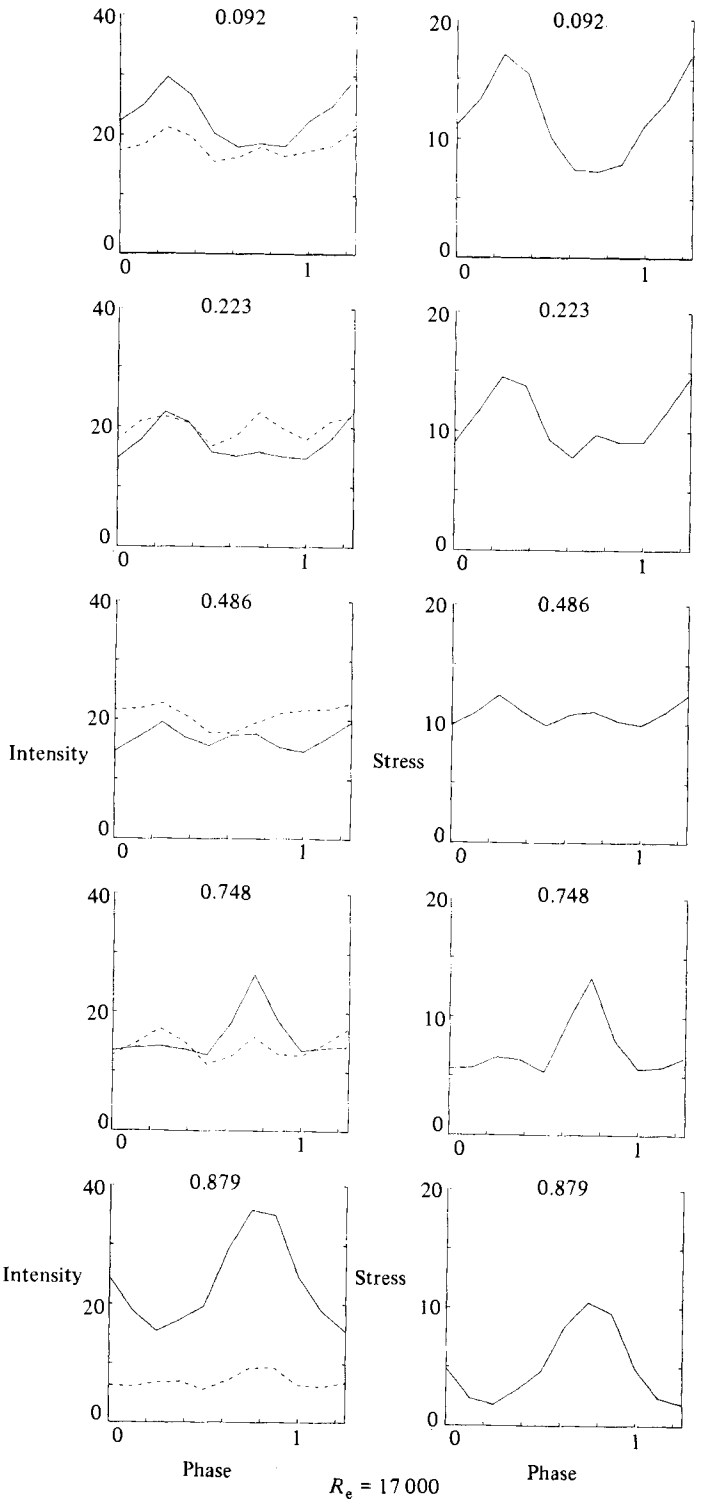

FIGURE 7(*b*). For caption see p. 356.

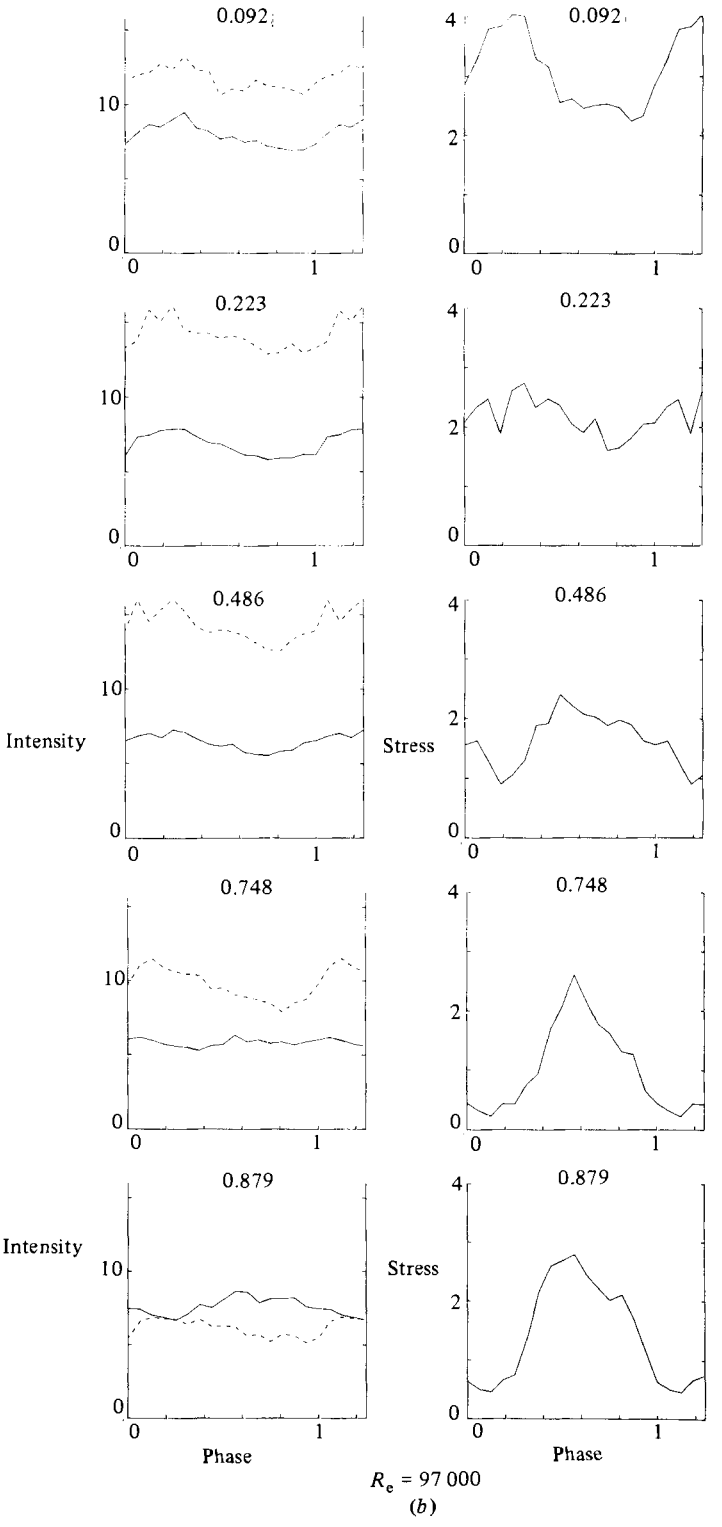

FIGURE 7. Conditional averages of 'small-scale' intensities and Reynolds stress against cycle phase for a range of axial positions at Reynolds numbers of 17 000 and 97 000: (*a*) intensities of the axial and azimuthal components; (*b*) intensities of the radial and azimuthal velocity components and Reynolds stress of the small-scale motion. (Broken lines are v or w, numbers are gap ratios z/d.)

are small with two maxima, one for maximum outward velocity and one for maximum inward velocity. Note that the variations of Reynolds stress are proportionally much larger than those of intensities.

At the larger Reynolds number, the anemometer outputs were passed through filters of non-dimensional time constants about 0.8, a compromise value chosen to reduce contributions from fluctuations of orbital frequency without too much attenuation of small-scale turbulence. It may be seen that the intensities and stresses are considerably less than would be expected from the low-speed results, but again the fractional variations of Reynolds stress are much larger than those of the intensities. The variations are similar in form, and the differences in magnitude may be due to attenuation of the random component by the filters. It is possible that the distributions of intensity and stress within the large-scale motions are similar over the range of speeds investigated.

8. Dependence of large-scale eddy structure on Reynolds number

Over the range of Reynolds number 8500–120000 three changes are observed in the structure of the large eddies and in the turbulent flow.

(i) The (reversed) radial gradients of mean angular momentum are reduced by a factor of about 1.5 between $R_e = 8500$ and $R_e = 50000$ (Smith & Townsend 1982). The present measurements, though not designed to provide accurate values of mean velocity, confirm the trend to $R_e = 120000$.

(ii) Turbulent motion and mean flow in the wall layers change from being completely dominated by dynamical effects of flow curvature to having an appreciable region of 'wall turbulent flow' relatively unaffected by the curvature.

(iii) The large eddies change in form from extremely regular toroids to less regular, possibly segmented, helical eddies. Their velocity scales, expressed as fractions of the friction velocity, may not decrease significantly.

The velocity distribution in an helical eddy can be regarded as the linear superposition of two azimuthal modes, symmetrical with respect to the axial direction, i.e.

$$v = \frac{C'}{r}\cos\left(\frac{\pi z}{d}\right)\cos(ky-\theta)$$

$$= \frac{C'}{r}\cos\left(\frac{\pi z}{d}\right)\cos ky\cos\theta + \frac{C'}{r}\cos\left(\frac{\pi z}{d}\right)\sin ky\sin\theta, \tag{8.1}$$

and, since the toroidal eddies are similar to the first laminar, axisymmetric mode of instability, it seems possible that the changes in velocity pattern are associated with changes in the effective 'turbulent' Taylor number for the central part of the flow where the motion is dominated by the effects of flow curvature.

Although the form of the Taylor number for a stationary outer cylinder conceals it, the number is descriptive of a flow with two distinct scales of velocity, one specifying the overall variation of angular momentum, the other the rate of flow curvature, with two functions for the fluid viscosity, axial diffusion of angular momentum and energy dissipation of the motion in the axial and radial directions. By assuming flow similarity in the outer parts of each wall layer, i.e. that the motion is determined by the transmitted torque, the rate of flow curvature and distance from the flow boundary, the two scales can be found by the analogy between Couette flow and Bénard convection. In the analogy, the temperature coefficient of buoyancy αg corresponds to $2U/r^2$, the buoyancy flux with the flux of angular momentum

$\overline{uw}\,r = G/r$, and the mean temperature with mean angular momentum Ur. If the variation of $2U/r^2$ can be ignored, dimensional arguments show that the variation of Ur over the region of strong flow curvature is a multiple of $G^{\frac{1}{2}}$. Then, by analogy with the Rayleigh number for Bénard convection, the Taylor number is

$$T_{\text{eff}} = \frac{2U}{r^2}\frac{d^3G^{\frac{1}{2}}}{\nu_s \nu_d}, \tag{8.2}$$

where ν_s is the eddy viscosity describing energy transfer from the toroids or helices to the small-scale turbulence, and ν_d is the eddy diffusion coefficient for axial variations of angular momentum.

To find the dependence of the eddy viscosity and the eddy diffusivity on the flow parameters, scale velocities and scale lengths must be found characteristic of the small-scale motions that transfer energy and momentum. Because the turbulent motion itself may be strongly influenced by the flow curvature, the choice is not as straightforward as in unidirectional flows. For large Reynolds numbers, rates of shear for the smallest eddies of the dissipation chain greatly exceed the rate of flow curvature, and the distribution of energy among eddies of different sizes is given by the Kolmogorov spectrum

$$E(k) = C\epsilon^{\frac{2}{3}}k^{-\frac{5}{3}}, \tag{8.3}$$

where ϵ is the rate of energy dissipation, and k^{-1}, the inverse of the wavenumber, specifies eddy size. The distribution can be valid only for eddy sizes small compared with those containing most of the turbulent energy, and also sufficiently small that their velocity gradients are large compared with the rate of flow curvature. The last condition may be expressed as $k \gg k_c$, where

$$k_c = \epsilon^{-\frac{1}{2}}\left(\frac{U}{r}\right)^{\frac{3}{2}}. \tag{8.4}$$

In the central region of nearly constant Ur, flow energy is transferred to the turbulence at a rate $2GU/r^3$, and the rate of energy dissipation should be of comparable magnitude. Omitting all constants of order one,

$$k_c = U_1/G^{\frac{1}{2}} \tag{8.5}$$

and $k_c d = (d/R_1)C_f^{-\frac{1}{2}} \approx 15$, implying that the effect of flow curvature is small only for eddies considerably less in size than the flow width. The turbulence spectra reported by Smith & Townsend have median wavenumbers near $kd = 12$ for low speeds, and the nearly isotropic spectrum begins at a similar wavenumber for $R_e = 100000$.

Curvature effects in flows with nearly irrotational mean flow commonly lead to generation of long Görtler eddies with axes and vorticity nearly parallel with the flow. Fully three-dimensional eddies are not expected for eddies of size greater than k_c^{-1}, and energy transfer and momentum diffusion is expected to be weak, the main effect of the Görtler eddies being to convect without irreversible mixing. Then the main energy transfer is to eddies of sizes in the region of k_c^{-1}.

The velocity scale for eddies of that size is $\epsilon^{\frac{1}{3}}k_c^{-\frac{1}{3}}$, and so the eddy viscosity ν_s is of magnitude

$$A_s\epsilon^{\frac{1}{3}}k_c^{-\frac{4}{3}} = \frac{A_s G}{U_1 R_1}, \tag{8.6}$$

where A_s is a constant near one. Putting ν_d equal to the product of friction velocity $\tau_1^{\frac{1}{2}}$ and flow width, i.e. $(G/U_1R_1)(d/R_1)$, the turbulent Taylor number becomes

$$T_{\text{eff}} = A_s^{-1} C_f^{-\frac{3}{2}} \left(\frac{d}{R_1}\right)^3. \tag{8.7}$$

Over the range of Reynolds number 17000 to 120000, the turbulent Taylor number changes in the ratio 1.63:1 (assuming friction coefficient proportional to $R_e^{-\frac{1}{4}}$†), a change that could be sufficient for development of a higher-order mode of instability in the viscous laminar flow. Coles (1965) found that the first 'wave' mode appeared in his apparatus at a Taylor-number ratio of 1.55 for a radius ratio of 1.144, which is much less than 1.5, the ratio in use.

No account has been taken of possible changes in the boundary conditions at the edges of the central, curvature-dominated flow. The conditions should be that normal velocity is zero and that slow velocity changes in the axial and circumferential directions cause stress fluctuations of nearly

$$v\frac{\mathrm{d}(G/r^2)}{\mathrm{d}U} \approx v\frac{G}{U_1 R_1^2}, \tag{8.8}$$

where v is the velocity fluctuation. If the stress changes in the central flow due to toroidal eddies are described by the eddy viscosity ν_d, changes in surface stresses will be in fixed proportion to them.

9. The radial distribution of mean angular momentum

In §8 it was argued that only the small-scale eddies of the turbulent motion (with wavenumbers more than k_c defined by (8.4)) can be fully three-dimensional and relatively unaffected by the curvature and strain rates of the mean flow. Their action on the mean flow and on the larger Görtler-type eddies is to transport momentum down velocity gradients while the larger eddies diffuse and equalize angular momentum. The larger eddies, being of considerable extent in the flow direction and so with small pressure gradients, move fluid around while conserving the angular momentum, and their equalization of differences in angular momentum is opposed by the tendency of the small, more nearly isotropic, eddies to produce a condition of solid-body rotation. From that qualitative description of the roles of the two kinds of eddy, it appears that radial gradients of angular momentum near the flow centre should lie between zero and $2U$, the value for solid-body rotation. If the eddy diffusivity for angular momentum is proportional to the product of friction velocity and flow width, values of the non-dimensional gradient $U_1^{-1}\,\mathrm{d}(U_1 r)/\mathrm{d}r$ should be a multiple of the ratio of the eddy viscosity for momentum transport to that eddy diffusivity. The ratio is proportional to $C_f^{\frac{1}{2}}$.

A similar result may be reached by assuming gradient diffusion near the centre of the annulus, with eddy transport coefficients ν_s for momentum and ν_d for angular momentum. Then the equation (3.1) for flux of angular momentum becomes

$$G = -\nu_d r\frac{\mathrm{d}(Ur)}{\mathrm{d}r} - \nu_s r^3 \frac{\mathrm{d}(U/r)}{\mathrm{d}r}, \tag{9.1}$$

† Levels of turbulent intensity in the flow are so large – around 15% – that Reynolds stresses cannot be measured with sufficient accuracy to determine closely the dependence of friction coefficient on Reynolds number. The assumed dependence as $R_e^{-\frac{1}{4}}$ is broadly consistent with the available measurements.

which can be rearranged as

$$\frac{1}{U_1}\frac{\mathrm{d}(Ur)}{\mathrm{d}r} = -\frac{G}{U_1 r(\nu_s+\nu_d)} + \frac{2\nu}{U_1}\left(\frac{\nu_s}{\nu_s+\nu_d}\right). \tag{9.2}$$

Approximating the second term by using $Ur \approx \frac{1}{2}U_1 R_1$, and with a value for ν_s of $A_s G/(U_1 R_1)$ (see (8.6)),

$$\frac{1}{U_1}\frac{\mathrm{d}(Ur)}{\mathrm{d}r} = \frac{\nu_s}{\nu_s+\nu_d}\frac{R_1}{r}(1-A_s). \tag{9.3}$$

If ν_d is of order $G^{\frac{1}{2}}d/R_1$, i.e. the product of the friction velocity $\tau_1^{\frac{1}{2}}$ and the flow width, ν_s is less than ν_d by a factor of $C_f^{\frac{1}{2}}$, and the non-dimensional gradient of Ur becomes

$$\frac{d}{U_1 R_1}\frac{\mathrm{d}(Ur)}{\mathrm{d}r} = O(C_f^{\frac{1}{2}}) \tag{9.4}$$

Distributions of angular momentum reported by Smith & Townsend (1982) have central gradients of 0.07 for $R_e = 8500$ and of 0.05 for $R_e = 50000$. These values are similar in their magnitude and ratio to the values of $C_f^{\frac{1}{2}}$, 0.040 and 0.033 respectively, supposing the friction coefficient to vary as the inverse fourth power of the Reynolds number.

10. Effects of the axial flow on the large eddies

For Reynolds numbers below 30000, the large eddies are toroidal in form and remarkably uniform in scale velocity and axial spacing. Reduction of the slow axial flow from the standard value of (approximately) $0.003U_1$ to $0.0010U_1$ has no appreciable effect on the velocity pattern, perhaps not unexpectedly since the axial pitch of the mean flow is 12 mm for the standard condition, small compared with the periodic spacing of the toroids, 150 mm. The regularity of spacing and scale velocity is remarkable since the toroidal eddies form at the entrance of the annulus distant only six periodic spacings from the measurement stations. Apparently, the configuration of toroidal eddies equally spaced is very stable, and flow patterns formed at the entrance rapidly approach the equilibrium configuration.

Changes in the axial flow have a considerable effect on the large eddies for Reynolds numbers above 50000. For the standard flow, the velocity patterns near the outer cylinder can be described to a first approximation by distributions of form

$$v_s = a\cos ky + b\cos(ky-\theta) \tag{10.1}$$

convected axially with velocity $V_c = 0.003U_1$. The velocity pattern is composed from a toroidal eddy of velocity scale a added to a 'single-start' helical eddy of scale b, the ratio b/a increasing with Reynolds number. The sense of the helical component is the same as that of the mean flow helix, as was shown by reversing the direction of axial flow. At the highest Reynolds number, the helical component becomes dominant.

For the reduced axial flow, $V_c \approx 0.0010U_1$, the relative intensity of the azimuthal (helical) mode is less at similar Reynolds numbers, and the distribution is better described by

$$v_s = a\cos ky + b\cos ky\cos\theta. \tag{10.2}$$

The second distribution may be described as that of a toroidal eddy with circumferential modulation of velocity, becoming for large values of b/a a toroid divided

circumferentially into two equal parts of opposite rotation. While there may be some residual helicity, it is much less than for the standard axial flow and the ratio b/a is much smaller.

Comparison of the autocorrelations $R(\tau)$ for the two axial velocities shows that the coherences (neglected in the approximate descriptions of (10.1) and (10.2)) for the toroidal components are similar but that the coherence of the helical component is of longer duration than that of the symmetrical component $\cos ky \cos\theta$. The difference may be that toroidal eddies are not interrupted by velocity nodes and are more stable and well-defined than symmetrical modes with two nodes. The smaller amplitude of the symmetrical mode indicates that, if the axial velocity is sufficient to induce the helical form, the helical mode is decidedly the more unstable and able to extract energy from the mean flow.

In spite of the considerable differences in the large-scale flow, conditional averages of velocity fields show that the radial variations of velocity are related to the local flow at the outer cylinder in similar ways for both axial velocities.

11. Concluding remarks

At the start of the experiments, it seemed reasonable to assume that an axial flow less than 0.015 of the circumferential flow velocity could have little effect on the motion, apart from moving large-scale eddies past fixed sensors. The first evidence to the contrary was the change in the large eddies from the toroidal form to the helical as Reynolds number increased from 50000 to 100000. That might be regarded as the development of secondary, azimuthal modes of flow instability biased towards a helical form to conform better with the helical path of the mean flow except for the measurements of autocorrelation with reduced axial flow. If the effect were simply to select one of two modes that are equally likely in the absence of flow, the large-scale motion with reduced flow would be expected to differ only in the proportion of the azimuthal modes and not on their total intensity. Autocorrelations at Reynolds numbers near 100000 (figures 2 and 3) show that the proportions do change but that their intensities become much less with reduced axial flow, while the toroidal mode is much stronger.†

Spectra reported by Smith & Townsend (1982) for axial flows similar to those of the present work show very large changes in form occurring over the range of Reynolds numbers 20000–100000, indicating development of strong Görtler eddies in the central flow of lengths ranging from one half-circumference to about a flow width. The changes in spectra and in large-eddy form are so large as to suggest that the flow has been steered by the axial flow into a new configuration, distinct from that existing for small or zero axial flow. Measurements of spectra with small axial flows could show whether the Görtler eddies occur only with the helical flow. If they are not found with small axial flows, that would be evidence that the flow configuration may be drastically changed by an apparently weak axial flow.

One minor observation should be mentioned. The variations of turbulent intensities within the velocity patterns of the large eddies, whether the toroidal eddies at smaller Reynolds numbers or the helical ones at larger Reynolds numbers, are proportionally much less than those of the Reynolds stress (figure 7), with ratios in excess of 2:1. The behaviour is found with both methods of phase determination. Comparable variations in the ratio of Reynolds stress to total turbulent intensity are not found

† Calculations of Davey, Di Prima & Stuart (1968) indicate the possibility of helical ('spiral') modes appearing as an instability of the toroidal eddies.

in unidirectional flows with no reversal in sign of the stress, and the effect poses an interesting problem. I can only surmise that turbulent fluid generated in the strong shear gradients in the wall layers undergoes considerable structural changes as it is exposed to the irrotational distortion in the central flow.

REFERENCES

BARCILON, A., BRINDLEY, J., LESSEN, M. & MOBBS, F. R. 1979 *J. Fluid Mech.* **94**, 453.

BOUABDALLAH, A. & COGNET, G. 1980 In *Laminar–Turbulent Transition* (ed. R. Eppler & H. Fasel), p. 368. Springer.

COLES, D. 1965 *J. Fluid Mech.* **21**, 385.

DAVEY, A., DI PRIMA, R. C. & STUART, J. T. 1968 *J. Fluid Mech.* **31**, 17.

DI PRIMA, R. C. & SWINNEY, H. L. 1981 In *Hydrodynamic Instabilities and the Transition to Turbulence* (ed. H. L. Swinney & J. P. Gollub), p. 139. Springer.

GOLLUB, J. P. & SWINNEY, H. L. 1975 *Phys. Rev. Lett.* **35**, 927.

KOSCHMIEDER, E. L. 1979 *J. Fluid Mech.* **93**, 515.

SMITH, G. P. & TOWNSEND, A. A. 1982 *J. Fluid Mech.* **123**, 187.

SMITH, G. P. & TOWNSEND, A. A. 1983 In *Structure of Complex Turbulent Flows* (ed. R. Dumas & L. Fulachier), p. 185. Springer.

ZAMAN, K. B. M. Q. & HUSAIN, A. K. M. F. 1980 *J. Fluid Mech.* **101**, 449.